ST. ANTHONY FALLS HYDRAULIC LABORATORY
UNIVERSITY OF MINNESOTA

Project Report No. 66

FORCE CHARACTERISTICS OF FLAPPED, VENTILATED HYDROFOILS IN SMOOTH AND ROUGH WATER

Submitted by
LORENZ G. STRAUB
Director

Prepared by
J. M. WETZEL and W. H. C. MAXWELL

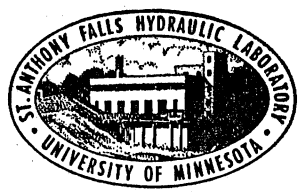

January 1963

Prepared for
OFFICE OF NAVAL RESEARCH
Department of the Navy
Washington, D.C.
under
Project NR 062-286, Contract Nonr 710(47)

PREFACE

Considerable experimental and theoretical information concerning flapped airfoils is available in aerodynamic literature. A hydrofoil with a flap operating in a non-cavitating condition would be expected to behave similarly to the airfoil. Some theoretical work has been done for the supercavitating hydrofoil with flaps, although it has previously been limited to the study of two-dimensional foils at zero cavitation number. It was the purpose of this investigation to obtain experimental data on the force characteristics of flapped, ventilated hydrofoils of finite span in smooth water for non-zero cavitation number, and also to determine the oscillatory forces on a restrained, artificially ventilated foil moving through a regular wave train.

The study was conducted during the period November 1, 1961 to January 31, 1963 under terms of Office of Naval Research Project NR 062-286, Contract Number Nonr 710(47).

Numerous members of the Laboratory staff assisted in various aspects of the program. C. E. Bowers critically reviewed the report. F. R. Schiebe was primarily responsible for the development of the instrumentation, and also is to be thanked for his many stimulating discussions. The bulk of the experimental data was due largely to the efforts of L. Boyer. The report was prepared for publication by Carol Takyi under the general supervision of Loyal Johnson.

A B S T R A C T

Experimental measurements were made of the lift and drag forces on superventilated hydrofoils of finite span submerged below a free surface. The foils were equipped with fixed trailing edge flaps of various angles of deflection. Experimental lift data taken with the foil in smooth water and extrapolated to zero cavitation number agreed well with two-dimensional theory modified to include effects of finite span and submergence.

Measurements of the oscillatory forces for an artificially ventilated foil moving through a regular progressive wave train agreed well with quasi-steady calculations for near zero σ. At the higher σ, the calculated values were greater than the measured, primarily through deficiencies in the prediction of the oscillatory cavity pressure.

C O N T E N T S

LIST OF ILLUSTRATIONS

LIST OF SYMBOLS

A - constant in conformal transformation, also area of body between separation points

AR - aspect ratio

a - constant in conformal transformation, also wave amplitude

c - hydrofoil chord

c_a - concentration of voids by volume in reentrant jet

c_f - flap length

c_w - wave celerity

C_L - lift coefficient

C_D - drag coefficient

d - non-dimensional distance from leading edge to flap hinge

$\bar{d}$ - distance in transformed hydrofoil plane corresponding to d

f - submergence of leading edge of foil below free surface

g - acceleration of gravity

K - reduced frequency, $\frac{\nu c}{2V}$

k - $2\pi/\lambda$

m - lift curve slope

P - ambient pressure in free stream

P_c - measured cavity pressure

R - gas constant

T - absolute temperature

t - time

u - horizontal component of wave orbital velocity

$\bar{u}$ - non-dimensional velocity, u/V

V - towing velocity

W - air-flow rate into cavity, lb per sec

w - vertical component of wave orbital velocity

$\bar{w}$ - non-dimensional velocity, $\frac{w}{V}$

α - geometric angle of attack

α_c - angle of attack due to camber

α_e - effective angle of attack, $\alpha_{eq} + \alpha_c$

α_{eq} - angle of attack of an equivalent flat plate

α_i - induced angle of attack

γ - specific weight

δ - flap angle

η - water surface elevation

θ - arbitrary angle

λ - wave length

ν - frequency of encounter

ρ - fluid density

σ - cavitation number

τ - planform correction factor

ϕ - phase lead

ω - circular frequency

Subscripts:

D - refers to drag

g - refers to geometric measure

L - refers to lift

m - refers to maximum value, i.e. amplitude

o - refers to steady conditions in smooth water

p_c - refers to cavity pressure

w - refers to conditions in waves

σ - refers to cavitation number

FORCE CHARACTERISTICS OF FLAPPED VENTILATED FOILS IN SMOOTH AND ROUGH WATER

I. INTRODUCTION

General operation of hydrofoil craft utilizing supercavitating or ventilated foils of zero dihedral angle as lifting surfaces will normally require some type of lift control. In either aerodynamics or in the wetted flow (noncavitating) operation of hydrofoils, trailing edge flaps of some form are commonly used as lift control devices. These flaps may also be used for ventilated foils, although they are effective only for increasing the lift as the upper surface of the foil is usually enclosed in the cavity itself. As the flap is deflected, the lift will increase correspondingly, and the drag will also increase.

Several theoretical analyses have been published concerning the supercavitating two-dimensional hydrofoil with flaps for zero cavitation numbers. Tulin [1] used linearized theory to determine the force characteristics for the foil in an infinite fluid. His work was more recently modified by Auslaender [2] to include the effects of the free surface. Auslaender also used linearized theory in his analysis. Lin [3] resorted to free streamline theory to calculate the forces on the foil for the infinite fluid case. All the theories were based on the assumption of zero cavitation number and no exact theory is known to exist at the present time for foils operating near a free surface at an arbitrary cavitation number.

One of the primary interests in the current investigation was to determine the force characteristics of flapped, ventilated foils of finite span at various cavitation numbers. This information was used to determine the validity of theory modified to include the effects of finite span, as well as in the calculation of the quasi-steady oscillatory forces on a restrained ventilated foil moving through a regular wave train. Considerable work of a similar nature has been done previously for noncavitating flows, and results of these studies have been published in various papers [4, 5]. In general, the studies for noncavitating flows conducted in regular waves indicated that effects of unsteadiness were of such magnitude that quasi-steady theory was not adequate except for very low reduced frequencies. At

a given velocity these low frequencies would occur for the long wave lengths in head seas, or in general at all wave lengths in following seas. It was conjectured that artificially ventilated foils may behave somewhat differently, particularly for cavities of the reentrant jet type. Therefore, a series of experiments was performed to first determine the force characteristics of a ventilated foil in smooth water, and second to determine the oscillatory force characteristics of a restrained foil moving through a regular progressive wave train. The tests were conducted with foils of finite span in the vicinity of the free water surface. The work was sponsored by the Office of Naval Research under terms of Contract Nonr 710(47).

II. GENERAL CONSIDERATIONS

Rather vast quantities of literature are available pertaining to the force characteristics of an airfoil equipped with flaps. The theory developed for airfoils may be applied generally to deeply submerged, noncavitating hydrofoils. The lift coefficient for a flapped foil in smooth water may be written

$$C_L = \frac{\partial C_L}{\partial \alpha} \alpha_e + \frac{\partial C_L}{\partial \delta} \delta \qquad (1)$$

where α_e = effective angle of attack

and δ = flap angle

Experimental studies with noncavitating hydrofoils in smooth water have been performed at Convair, and reported by Jones [6]. He found that the lift curve slope, $\partial C_L/\partial \alpha$, was essentially independent of flap deflection. The term, $\partial C_L/\partial \delta$, is commonly called the flap effectiveness, and in aerodynamics is a function of the ratio of the flap chord to foil chord, and of the ratio of the flap span to foil span. For a hydrofoil near the free water surface, the flap effectiveness may also be expected to be a function of the foil submergence. Calculations considering the variation with submergence were described in Jones' paper, and the experimental data indicated that the predicted flap effectiveness using airfoil theory techniques was considerably greater than that measured.

With a supercavitating foil, the general relationship for the lift coefficient in Eq. (1) would also be expected to be valid, except that the

variation of the lift coefficient with cavitation number must also be considered. Theoretical work for zero cavitation number and two-dimensional foils is described in Refs. [2] and [3]. For a foil ventilated by injecting gas onto the upper surface of the foil or directly into an existing cavity, the cavitation number can be varied to some extent by exercising control over the cavity pressure. It is well known that for steady flow, ventilated cavities are similar to natural cavities in most respects. Exceptions, such as pulsation of the cavity, may arise from the introduction of excessive quantities of gas. However, with unsteady flows such as experienced by a foil moving through a regular progressive wave train, considerable differences may exist. For a natural cavity, the cavity pressure would remain essentially constant (vapor pressure) for all conditions. For an artificially ventilated cavity, the cavity pressure would vary, with the magnitude of this variation depending largely upon the cavitation number or the cavity characteristics in the steady condition. Thus, the variation in cavity pressure is directly associated with the air-entrainment processes of ventilated flows. Basic studies of ventilated flows for various bodies have been conducted at this Laboratory [7, 8, and 9] and it may be advantageous to briefly discuss some of the major features of the ventilation phenomenon at this time. The relationship between air-entrainment rate and cavitation number was divided into two regions, one characterized by reentrant jet cavities, and the other by non-reentrant jet cavities. In the former region, the cavitation number was essentially proportional to the air-entrainment rate. In the latter region, the cavitation number was essentially independent of the air supplied to the cavity. Separating these two regions was a transition zone, that usually occurred at a cavitation number of approximately 0.1. The air-entrainment rate for a reentrant jet cavity was a function of angle of attack, velocity, camber, and cavitation number. A correlation parameter was described in Ref. [7] that would satisfactorily reduce all data taken in the SAF towing tank facility to a common line. The air-entrainment rates for the reentrant jet cavities could be determined from the equation

$$W = \frac{c_a}{1 - c_a} \; \frac{\rho V^3 A C_D \sigma_v \left[1 - \frac{\sigma}{\sigma_v}\right]}{4RT\left[1 + \sqrt{1 + \sigma}\right]} \qquad (2)$$

where W = air-entrainment rate

C_D = drag coefficient

A = area of body between separation points

R = gas constant for air

T = absolute temperature of gas in cavity

V = free stream velocity

σ = cavitation number based on cavity pressure

σ_v = cavitation number based on vapor pressure

ρ = density of water

c_a = correlation parameter or concentration of voids by volume in the reentrant jet

The parameter, c_a, could not be determined directly. Therefore, using measured values of the other parameters in the equation, an empirical expression was determined for c_a. This expression was written as

$$c_a = 0.59 - 1.325\sigma + 0.0825\,AR\sigma \quad \text{for } 2.5 \leq AR \leq 6 \tag{3}$$

The concentration or correlation parameter can be seen to be independent of foil submergence, angle of attack, velocity, or camber. In the current tests it was desired to determine the validity of Eq. (3) for flapped foils, i.e. with foils of large camber. Again by using measured values of the other variables, the concentration was calculated. It will be shown in Section IV B that for the tests conducted at this Laboratory Eq. (3) may also be used for flapped foils.

If the air supply rate to a ventilated foil is held constant as the foil moves through a wave train, the cavity pressure will vary with respect to time. Assuming that the instantaneous cavity pressure is the same as the cavity pressure at the instantaneous geometric conditions, Eq. (2) may be applied to this case. The drag coefficient, C_D, is essentially a function of angle of attack, flap angle, and cavitation number for a given foil shape. At the present time, however, it is not possible to calculate the drag coefficient for a finite span foil at an arbitrary cavitation number. Instead, an empirical equation for C_D (as a function of angle of attack and cavitation number for a fixed flap angle) based on experimental data may be used. Substitution of this empirical expression for C_D in Eq. (2) results in a relation between angle of attack and cavitation number for a given air-flow rate, flap angle, and velocity. As the variation in angle of attack is known from the vertical component of the orbital velocity of the wave, the

change in cavitation number can then be found. This procedure would be valid only for reentrant jet cavities, as the use of Eq. (2) is restricted to that case. For the higher air-flow rates and non-reentrant jet cavities, the basic behavior of the air-entrainment process is such that the change in cavitation number with angle of attack may be expected to be rather small. Experimental evidence of this conclusion is presented in Section IV B.

III. EXPERIMENTAL APPARATUS AND PROCEDURE

A. Towing Facility

The tests were carried out in the St. Anthony Falls towing facility which consists of a tank 220 ft long, 9 ft wide, and 6 ft deep. The self-propelled towing carriage can reach speeds up to a maximum of 25 fps, although the length of test run at the top speed was not adequate for these particular tests and speeds were limited to 18 fps. The tank is equipped with a wave generator capable of producing regular waves of 3 to 40 ft in length and a maximum height of about 2 ft. A permeable beach absorber is located at the opposite end of the tank to minimize wave reflections.

B. Foils and Instrumentation

Flat plate foils of 3-in. chord, zero dihedral angle, and rectangular planform were used for all the tests. Foils with spans of 12 and 18 in. were available, resulting in aspect ratios of 4 and 6, respectively. These were utilized for the conditions shown in Table I of Fig. 1. The foils had a wedge cross section with a 6-degree angle, and were attached to a streamlined strut of 2-in. chord at midspan (see Fig. 1). A rabbet was machined over the entire span on the under side of the foil near the trailing edge. Fixed flaps were machined to fit into this rabbet, with flap angles of 0, 4, 6, 8, 12, 16, and 20 degrees for flap chord to foil chord ratios, c_f/c, of 0.25 and 0.50. The flaps were attached to the foil with screws, and the under surface was made smooth with body putty after the installation of each flap. The flap angle, δ, was measured with respect to the under side of the foil. The angle of attack, α, was defined as the angle between the velocity vector and the under side of the foil excluding the flap.

A circular depression was machined in the upper surface of the foil at about the quarter-span point aft of the mid-chord. This depression was

connected to a small tube laid in the foil and passing through the strut, the tube terminating in a connector suitable for attachment to a Statham pressure transducer. The circular depression in the foil was covered with a thin flexible diaphragm and the entire system was filled with liquid. This system was then used to measure average cavity pressures. The cavities were of such length that the diaphragm was always within the cavity.

As the speed of the carriage was not sufficient to obtain natural cavitation on the foil, it was necessary to supply air to the upper surface of the foil to force ventilation. The air was fed through the strut, and ejected along the span through ports at the base of the strut. A small quantity of air was also injected near the leading edge of the foil through a small tube extending into that region. This permitted satisfactory ventilation at lower angles of attack than could be obtained without the use of the supplementary air port. The air-flow rates were measured with a calibrated orifice meter placed in the air supply line.

The strut and foil assembly was attached to a device to permit adjustment of angle of attack, which in turn was mounted on a two-component dynamometer. The dynamometer was of a strain gage type, and simultaneous measurements of lift and drag could be made. The signals from the dynamometer, along with those from the pressure transducer and the velocity meter (tachometer generator) of the towing carriage, were recorded with a four-channel Sanborn recorder.

C. Procedure

For the series of tests in regular waves, the wave profile was measured with a sonic wave transducer developed at this Laboratory [10]. The sonic head of the transducer was mounted directly opposite the mid-chord position of the foil, and at a sufficient lateral distance from the foil to be unaffected by the disturbance created either by the foil or strut. For these tests the signal from the wave transducer was continuously recorded. Waves with lengths of 3 to 30 ft and a constant amplitude of 0.15 ft were used for most tests. The variation of cavity pressure due to the waves was measured by placing the diaphragm of a Consolidated pressure transducer directly into the cavity. A limited number of measurements were made in this manner, as the transducer was damaged during the course of the tests and repair could not be made in time for further investigations.

A typical record for a ventilated foil moving through regular head seas is shown in Fig. 2. Each of the traces is identified for reference purposes. Note that increasing drag is in the opposite direction to the increasing values of the other traces. Capacitors were used to eliminate some of the extraneous noise in the drag record of Fig. 2, and the data were corrected to account for these capacitors. Phase relationships between the cavity pressure, lift force, and the wave were also measured. The phase angle was defined as the number of degrees of wave cycle that the maximum value of the trace in question led the crest of the wave. Since little harmonic distortion appeared to exist in the records, the maximum amplitude of the oscillatory forces was used in data reduction.

IV. DISCUSSION OF RESULTS

A. Force Coefficients for Foil in Smooth Water

The force data were reduced in terms of the standard lift and drag coefficients based on the planform area of the foil. As the forces depended on both the angle of attack, α, and flap angle, δ, the notation $C_L(\alpha,\delta)$ or $C_D(\alpha,\delta)$ was adopted. Thus, the lift coefficient for a foil at $\alpha = 10$ degrees and $\delta = 4$ degrees was written $C_L(10,4)$. The forces also varied with cavitation number. The cavitation number, σ, was defined as

$$\sigma = \frac{P - P_c}{\frac{1}{2}\rho V^2}$$

where P = ambient pressure in free stream, psfa
P_c = measured cavity pressure, psfa
ρ = fluid density, slugs per cubic foot
V = velocity, fps

As the cavitation number was based on cavity pressure, no distinction was made between the cavitation number and the ventilation number as sometimes used in literature concerning ventilated cavities.

In an attempt to reduce the number of test runs required, it was first decided to determine the effects of velocity and submergence for a given angle of attack and flap angle. It can be seen from Fig. 3a and 3b

that the lift and drag coefficients varied only slightly with velocity over the range from 12 to 18 fps. The effect of submergence was investigated for 0.5, 1, and 2 chord submergences and is shown in Fig. 3c and 3d. Again little difference can be noted in the experimental data. The points calculated for $\sigma = 0$ are also shown. On the basis of these experimental results, most of the following tests were conducted at a submergence of 1 chord and a velocity of 16 fps. The typical variation of the force coefficients with angle of attack for a fixed flap angle is shown in Fig. 3e and 3f. The data for various angles of attack, flap angles, flap-chord ratios, and aspect ratios are plotted in Figs. 4 through 7 as a function of cavitation number. The effect of increasing the flap angle was to increase both the lift and the drag. The slopes of the curves appeared to be essentially independent of the flap angle for a given flap-chord ratio, c_f/c.

The two-dimensional non-linear theory by Lin for zero cavitation number has been modified by using the method of Johnson [11] to include the effects of finite aspect ratio and finite submergence. This modification is described in Appendix A of this report. The figures thus include the calculated value of the lift coefficient and the lift curve slope for $\sigma = 0$. The slope was obtained on the assumption that $C_L = C_{L_o} (1 + \sigma)$ for small σ, bearing in mind its limitations at low angles of attack (Wu [12]). The drag for $\sigma = 0$ was computed on the assumption that $C_D = C_L \tan \alpha_g$. This expression neglects skin friction effects as well as the deviation of the resultant force vector from the normal due to camber effects.

In the cases where the theoretical lift coefficient and lift curve slope at $\sigma = 0$ could be matched with the curves through the experimental data a continuous curve has been drawn; where this was impossible the curve was drawn through the data only and the computed value at $\sigma = 0$ indicated. The lack of data for the range $0 < \sigma < 0.04$ arises because of the increased air demand required as σ approaches zero (see Fig. 9a). The wide range of air-flow rates for a small variation of σ in the non-reentrant jet region also accounts for the clustering of data at low σ.

Lift-drag ratios may be determined from theory for $\sigma = 0$ and from experimental data for $\sigma > 0$. Typical plots of the lift-drag ratios against lift coefficient as functions of the angle of attack and flap angle are shown in Fig. 7c and 7d. The solid lines are drawn through points representing constant angle of attack, and the broken lines are drawn through

points representing constant flap angles. Generally as both the angle of attack and flap angle increase, the lift-drag ratio decreases.

Experimental data were not available at $\sigma = 0$, due to the high air-entrainment rates at low σ. The slope of the C_L versus σ and C_D versus σ curves was generally influenced by the theoretically computed values of C_L and C_D for $\sigma = 0$ in the range $0 < \sigma < 0.10$. The experimental data of Fig. 7d are therefore presented for $\sigma = 0.10$, at which point the C_L and C_D versus σ curve slopes are generally fully determined by the available experimental data and not by the theoretical values at $\sigma = 0$. The completely theoretical determination at $\sigma = 0$ is presented in Fig. 7c for comparison since there are no available theoretical means of determining the behavior at $\sigma = 0.10$ at the present time.

By making cross-plots of the data shown in Figs. 4 through 7, information was obtained on the effectiveness of the flap, or the variation of lift with flap angle and flap-chord ratio. Results of calculations for $\sigma = 0$ are plotted in Fig. 8a, 8b, and 8c for given angles of attack and flap-chord ratios of 0.25 and 0.50. A slight non-linearity of the lift coefficient becomes more evident at the higher flap angles. The calculated flap effectiveness also is greater for the larger flap to chord ratio. As shown in Fig. 8c, the effect of increasing the submergence from 1 to 2 chords is to slightly decrease the lift coefficient for all but the highest flap angles.

The influence of cavitation number on the effectiveness of the flap is shown in Fig. 8d for an angle of attack of 10 degrees and flap to chord ratio of 0.25. The line for $\sigma = 0$ is shown for reference purposes, being identical to that of Fig. 8b. As the cavitation number increases, the lift coefficient generally increases for a given flap angle. Lines drawn through the experimental data all have essentially the same slope. Since the slope of these curves is a measure of the flap effectiveness it appears that the effectiveness of the flap was essentially independent of cavitation number, for cavitation numbers of 0.1 or higher.

B. Air-Entrainment Rates

As it was necessary to ventilate the foils to create artificial cavities for all the tests described in this report, measurements were also made of the quantity of air introduced to the upper surface of the foil for

various conditions. A typical plot of the variation of air-entrainment rates with cavitation number for a flapped foil at two angles of attack and several flap angles is shown in Fig. 9a. Note that the air-flow rate has been divided by the area of the foil in square inches for the ordinate of this plot. Regions for reentrant jet and non-reentrant jet cavities are roughly indicated on the figure. The actual transition region was somewhat difficult to define accurately. As the angle of attack was increased for a foil without a flap, the air quantity required to maintain a given cavitation number or cavity pressure in the reentrant jet region was also increased. The effect of deflecting the flap was to thicken the cavity and thus increase the air required to maintain the given conditions. The data at the higher flap angles were limited by the air supply available on the carriage. For reentrant jet cavities, the air entrainment was a function of cavitation number, angle of attack, and flap angle. From Eq. (2) it can be seen that velocity is also a factor which must be considered. Additional data on the air-entrainment rates have been tabulated in Appendix C.

The correlation parameter given by Eq. (3) in Section II was previously found to be independent of angle of attack, camber, and velocity. It was of interest in the current investigation to determine the validity of Eq. (3) for flapped foils. Using Eq. (2) and measured values of C_D, W, σ, and τ, the correlation parameter was calculated. Typical results of this calculation plotted as a function of σ are shown in Fig. 9b for several flap angles. The solid line was calculated from Eq. (3). It can be seen that the data for flap angles up to 20 degrees scatter reasonably close to this line for cavitation numbers as high as 0.3. Additional data reduced to this form have been tabulated in Appendix C. It appears that Eqs. (2) and (3) are also valid for flapped foils with reentrant jet cavities for the conditions utilized.

C. Cavity Stability

In the course of the experimental program, observations were also made of the stability of the ventilated cavity. Previous work at this Laboratory [7, 8] has indicated that pulsation of the cavity may occur under certain conditions. A theory has been developed for pulsating cavities in a vertical free-jet water tunnel [9]. This theory indicated that a free surface was necessary for pulsation to occur. For a ventilated foil running

near a horizontal free surface, the gravity field may also be a factor influencing pulsation. For some bodies, such as a disk normal to the flow, pulsation could not be found in these limited tests. Instead, for long cavities, the air left the cavity through large tubes extending from the rear of the cavity. The existence of these tubes was associated with an additional circulation due to the buoyancy of the cavity, which increased with increasing cavity thickness. Therefore for flapped foils running near the surface, the particular air-entrainment process may be dictated by the cavity thickness in that the buoyancy effect may override the tendency for pulsation. Visual observations of the cavity with flapped foils have indicated that pulsation would generally not occur for the higher flap angles used in this investigation. Rather, the cavity remained essentially stable for the high air-flow rates. More extensive work concerning the bounds of stability is currently being investigated under terms of a separate contract on ventilated flows.

It should also be mentioned that for certain conditions it was difficult to obtain a stable cavity in the reentrant jet region. This instability was not associated with a pulsation of the cavity walls, but a gradual shortening of the cavity length with time and therefore may be more properly considered a transient effect. The general procedure used for establishing artificial cavities was to supply a constant air-flow rate to the upper surface before and throughout the test run. In some cases during the acceleration period the cavity would be rather long, and gradually decrease in length over the remainder of the run. It was found that tendencies for such an instability or long transient could be significantly reduced by carefully controlling the method of introducing air into the cavity. For example, if the air was injected gradually into the cavity during the acceleration period until the desired air-flow rate was established, the cavity would remain essentially stable over the rest of the run. By this method it was thus possible to obtain reliable data for most of the reentrant jet cavities. Further investigations on this phenomenon are being conducted under the ventilation contract, but it is felt that this may be essentially a problem in technique to obtain ventilated cavities.

Another type of instability encountered was cavity wash-off that occurred in some instances as the ventilated foil moved through a regular wave train. Wash-off will be discussed in a later section.

D. Oscillatory Forces in Regular Waves

As a restrained, ventilated foil moves through a regular wave train the foil encounters variations in the angle of attack, velocity, and submergence. Data for a forced-ventilated foil moving through smooth water indicated that the force coefficients were essentially a function of the angle of attack, flap angle, and cavitation number. The effective angle of attack varies in waves due to the vertical component of orbital velocity. The cavitation number also changes for a constant air supply rate, as can be seen with reference to Fig. 9a. At a constant supply of air to the cavity in the reentrant jet region, the cavitation number increased with increasing angle of attack for a given flap angle. For a specified ambient pressure and velocity, this increase in cavitation number corresponded to a decrease in the cavity pressure. Thus, it may be expected from quasi-steady assumptions that the cavity pressure and angle of attack are out of phase by essentially 180 degrees for a ventilated cavity of the reentrant jet type.

Measurements were made of the oscillatory lift and drag on a restrained foil for several steady (average) cavitation numbers and a wide range of wave lengths. These data are shown in Figs. 10 and 11. The steady cavitation number, σ_o, is the cavitation number that would be obtained for a given air-flow rate for the foil moving through smooth water. This air-flow rate was held constant for the series of tests at each particular σ_o. The ordinate on the graphs is a ratio of the maximum amplitude of the oscillatory force coefficients to the wave amplitude. The reduced frequency, $\nu c/2V$, based on the chord, is also shown on the abscissae of Figs. 10a and 11d along with the wave length. The frequency of encounter, ν, is defined for head seas as

$$\nu = \frac{2\pi}{\lambda} (V + c_w)$$

where λ = wave length
V = velocity
c_w = wave celerity

As the data shown were taken for a given velocity, submergence, and wave amplitude, each wave length thus corresponds to a particular change in angle of attack due to the vertical component of orbital velocity. The angle

change therefore reduces with increasing wave length. Figures 10a, 10b, and 11a show data taken for a foil with no flap moving through regular head seas whose amplitude remained constant at approximately 0.15 ft. The geometric angle of attack of the foil was fixed at 10 degrees. The amplitude of the oscillatory lift coefficient attained a maximum value at a wave length in the vicinity of $\lambda = \pi$ and thereafter decreased with increasing wave length for each cavitation number. The amplitude increased with increasing cavitation number, primarily because the variation in cavitation number, $\Delta\sigma$, resulting from the variation in the angle of attack, $\Delta\alpha$, increases rapidly with σ_o. At the low σ_o, or high air-flow rates, it can be seen from the air-entrainment curves, such as shown in Fig. 9, that the change in cavitation number with angle of attack is quite small. Therefore, at the high flow rates the oscillatory lift depends essentially on the lift curve slope, $\partial C_L/\partial\alpha$, and the change in angle of attack, $\Delta\alpha$. For the lower air-flow rates and consequently higher σ_o, the change in σ with α is considerably greater. Thus the term $[\partial C_L/\partial\sigma](\Delta\sigma)$ becomes quite large, and is a large factor in the total oscillatory lift. The success of calculating the forces from a quasi-steady theory then lies in the ability to adequately predict the change in cavitation number, $\Delta\sigma$, for the reentrant jet cavities. An estimate of this change can be found by making a cross-plot of the air-entrainment rate versus cavitation number curves for a constant air-flow rate, thereby obtaining a relationship between angle of attack and cavitation number. The slope of this curve was very flat, indicating that even a relatively small change in angle of attack would result in a rather large change in cavitation number. The change in angle of attack was computed from the vertical component of the orbital velocity of the wave. For each wave length it was possible to calculate the expected change in angle of attack and, by neglecting dynamic effects on the cavity, the corresponding change in cavitation number as determined from the previously mentioned cross-plot.

Some data were also taken with the same foil at a 10-degree angle of attack and a flap angle of 16 degrees. These data are shown in Figs. 10c, 10d, 11b, 11c, and 11d. The addition of the flap caused a reduction in the amplitude of the oscillatory force coefficients for the higher values of σ_o. The flap addition causes a slight increase in $\partial C_L/\partial\sigma$ and an appreciable reduction in $\partial C_L/\partial\alpha$ for high σ_o. There is no appreciable change in the amplitude of the oscillatory force coefficients for low values of σ_o.

For higher values of σ_o and the larger flap angles the value of $\partial^2 C_L/\partial \alpha^2$ was found to be very large and negative. A non-linear analysis revealed that this contributed nothing to the fundamental response, its contribution being to the steady displacement and the second harmonic. It generally combined with other very small quantities and its overall influence was therefore small. For the 3 in. by 12 in. wedge flat plate moving through head seas of amplitude 0.15 ft at 16 fps with $\alpha = 10$ degrees, $\delta = 16$ degrees, $f = 1$ chord, $c_f/c = 0.25$ and $\sigma_o = 0.242$, and using smooth water values $C_{L_o} = 0.576$, $\left.\frac{\partial C_L}{\partial \alpha}\right|_o = 0.773$, $\left.\frac{\partial C_L}{\partial \sigma}\right|_o = 0.775$, $\left.\frac{\partial^2 C_L}{\partial \alpha^2}\right|_o = -16.27$, $\left.\frac{\partial^2 C_L}{\partial \sigma^2}\right|_o = 0$ and $\left.\frac{\partial^2 C_L}{\partial \alpha \partial \sigma}\right|_o = -0.466$, non-linear computations were made at the two wave lengths, $\lambda = 3$ ft and $\lambda = 30$ ft. The ratio of the steady displacement to the amplitude of the fundamental was found to be 0.055 at the 3-ft wave length and 0.0346 at the 30-ft wave length. The ratio of the amplitude of second harmonic to the amplitude of the fundamental was 0.0621 at the 3-ft wave length and 0.0388 at the 30-ft wave length. These computations were made for a condition at which $\left.\frac{\partial^2 C_L}{\partial \alpha^2}\right|_o$ was a maximum or close to a maximum for the range of tests reported.

Figures 10 and 11 include theoretical curves whose derivation is discussed in Appendix B. The theoretical curves computed from measured values of the change in cavity pressure in waves, ΔP_c, and the approximation for low σ agree well with the data for $\delta = 0$ degrees and agree fairly well for $\delta = 16$ degrees. The computation based on smooth water data gives very poor agreement with data, mainly because of the difficulty of accurately obtaining the $\Delta\alpha$ to $\Delta\sigma$ relationship discussed above. In effect this means that ΔP_c cannot be accurately predicted from smooth water data.

The α, σ relationship was obtained experimentally for an AR = 4 foil with $\alpha_o = 10$ degrees and $\delta = 16$ degrees, $c_f/c = 0.25$, $f = 1c$ at $\sigma_o = 0.188$. Values of $\left.\frac{\partial C_L}{\partial \alpha}\right|_o$, $\left.\frac{\partial C_L}{\partial \sigma}\right|_o$, and C_{L_o} were obtained by interpolation from the smooth water test data for various angles of attack, flap angles and cavitation indices (Fig. 4). This information was substituted in Eqs. (B-8) of Appendix B to obtain the curve of $\left|\frac{\Delta C_L}{a}\right|$ and ϕ_L against λ. The fact that the theoretical curve greatly exceeds the measured values at low wave lengths or high frequencies of encounter and slightly exceeds the measured values at the lower frequencies of encounter indicates that besides the other shortcomings of the method, unsteadiness effects may be quite significant.

For the theoretical curves obtained using measured values of cavity pressure amplitude and phase as discussed in Section C of Appendix B, good agreement exists between theory and data when $\delta = 0$ degrees. In the case of the 16-degree flap and at high frequencies of encounter the theoretical $\left|\frac{\Delta C_L}{a}\right|$ is much higher than the measured value whereas there is good agreement at low frequencies of encounter. It should be noted that the discrepancy is probably due to the application of Eq. (B-11) to flapped foils, rather than unsteadiness effects, in view of the apparent lack of unsteadiness effects for the case where $\delta = 0$ degrees.

The measured amplitude and phase of the cavity pressure for the foil moving through waves is shown in Fig. 11c and 11d. The computation of the change in cavity pressure expected to occur on the basis of the α, σ relationship obtained from smooth water data is also included. Its lack of agreement with the measured values again indicates the inadequacy of using the smooth water measurements for theoretical predictions in waves. The pressure data for $\sigma_o = 0.053$ and $\sigma_o = 0.158$ were obtained by placing the diaphragm of a pressure transducer directly through the side of the cavity; that for $\sigma_o = 0.242$ was obtained using the pressure diaphragm mounted flush with the upper surface of the foil as shown in the definition sketch (Fig. 1). The measurements for $\sigma_o = 0.053$ and $\sigma_o = 0.158$ are consequently of higher accuracy since some extraneous effects may be introduced in the $\sigma_o = 0.242$ case, where the pressure fluctuations were obtained from a remote transducer connected to the diaphragm by oil lines.

E. Phase Relationships

The phase relationship between the wave crest and the maximum forces or the cavity pressure was determined from the records whenever possible. Analysis of the experimental records indicated that the maximum lift led the wave crest, as shown in Fig. 10b and 10d for a foil with no flap and a foil with 16-degree flap at three average cavitation numbers. The phase lead generally decreased slightly with increasing wave length, and little difference in phase angle was noted for the three cavitation numbers. Observation of the records also indicated that the lift and drag forces were essentially in phase with each other in all cases, which was to be expected for a fully ventilated flow. The agreement between theoretical prediction and lift phase data is not completely satisfactory, with the exception of the prediction

based on smooth water data. It should be borne in mind that this method of prediction gave the greatest discrepancy between theoretical and experimental values of $\left|\frac{\Delta C_L}{a}\right|$ and $\left|\Delta P_c\right|$ so that the good agreement here is not particularly significant. In general, it is difficult to measure the phase relationships to a high degree of accuracy.

For the tests in which the diaphragm of the pressure transducer was placed directly into the cavity, reliable measurements of the cavity pressure phase relationships could also be made. These measurements are shown in Fig. 11d for a foil with a 16-degree flap for $\sigma_o = 0.053$ and 0.242. The data for $\sigma_o = 0.158$ were obtained from the remote pressure transducer connected to the diaphragm on the upper surface of the foil. The phase lead varied somewhat with wave length, from about 200-degree to 340-degree lead. The expected phase lead on the basis of quasi-steady assumptions would be about 270 degrees.

F. Cavity Wash-Off

Insufficient data were available to clearly delineate regions of wash-off from regions with no wash-off. For various angles of attack and wave amplitudes the wave length below which wash-off and reattachment of the cavity occurred was recorded. From these observations the general form of wash-off behavior could be inferred. A general summary of their implications is presented in Fig. 12. The shapes of the curves shown are not completely accurate and only give a general picture of the existing delineation. It is seen that for a low angle of attack the tendency for cavity wash-off at a given incident wave length tends to decrease with decreasing amplitude, and with increasing angle of attack. If the angle of attack is sufficiently high ($\alpha = 14$ degrees) there will be no wash-off at any amplitude (for $a < 0.2$ ft); if the amplitude is sufficiently small (0.1 ft) there will be no wash-off at any angle of attack ($\alpha > 8$ degrees).

The data available did not permit an accurate analysis of the dependence of wash-off on frequency of encounter, incremental velocity changes due to orbital motion caused by the waves, or wave steepness.

G. Cavity Characteristics in Waves

A brief investigation was made to determine the cavity characteristics of a ventilated foil moving through a regular wave train. In smooth

water the cavity length is a function of cavitation number, angle of attack, submergence, and aspect ratio. For a foil of zero dihedral angle, all parameters but the latter change due to wave motion. For a given cavitation number, the cavity length increases with increasing submergence and angle of attack. Of course, the cavity length also decreases with increasing cavitation number. For a ventilated foil operating at a low average σ_o, the change in σ is relatively small, but the relation between cavity length and σ is such that a considerable change in length may be expected. For a higher σ_o the change in σ may be large, but in this case a smaller change in cavity length may occur. It appears that the actual cavity length is a complicated function of the previously listed parameters.

A series of photographs was taken of the underside of a ventilated cavity in regular waves. The photographs could not be taken from directly above the foil as the surface waves created excessive distortion. A triggering device was mounted on the towing carriage rail to trip the camera shutter and also to mark the wave trace at the same instant. It was thus possible to relate each photograph to the location of the foil in the wave itself. Several of these photographs are shown in Fig. 13 for a wave length of 10 ft. The position of the foil in the wave at the instant the photo was taken is marked on the accompanying sketch of the wave profile. Double cavities are seen in the photographs. The lower cavity is the actual cavity and the upper one its reflection in the free surface. The reflected image shows the upper surface of the actual cavity. The location of the free surface is emphasized by the wake of the supporting strut. The first photograph in Fig. 13 is a photograph of a restrained flat plate foil at an angle of attack of 14 degrees moving through smooth water, and serves as a reference for the succeeding photos. The cavitation number was 0.14 for the smooth water case, and for the photos in the regular wave the mean cavitation number was essentially the same value. It can be noted from the photograph that the cavity was of the reentrant jet type. In several of the photographs the impingement of the reentrant jet on the lower surface of the cavity can readily be seen. It was not possible to obtain reliable cavity length measurements from this series of photographs taken at this oblique angle, but it appears that qualitatively some change in cavity length exists.

V. CONCLUSIONS

1. The increase in lift with a ventilated flapped foil varies linearly with the flap angle for a given cavitation number. The flap effectiveness also increased as the ratio of the flap chord to foil chord varied from 0.25 to 0.50.

2. The lift-curve slope, $\partial C_L/\partial\sigma$, for a given angle of attack was essentially independent of flap angle.

3. Qualitative agreement between experimental lift data extrapolated to $\sigma = 0$ and two-dimensional theory modified to include effects of finite span has been obtained for most flap angles.

4. Air-entrainment rates for flapped foils with reentrant jet cavities can be satisfactorily determined from Eq. (2).

5. Oscillatory lift forces on a restrained ventilated foil moving through a regular wave train can be predicted for cavitation numbers near zero (non-reentrant jet cavities) by using quasi-steady assumptions. Difficulty in predicting the variation of cavity pressure for the higher cavitation numbers and the associated reentrant jet cavities reduces the accuracy of the method.

6. The lift force leads the wave by about 70 degrees, and the lift and drag forces appear to be in phase with each other for essentially all conditions considered.

LIST OF REFERENCES

[1] Tulin, M. P. and Burkart, M. P. Linearized Theory for Flows about Lifting Foils at Zero Cavitation Number, DTMB Report C-638, 1955.

[2] Auslaender, J. The Behavior of Supercavitating Foils with Flaps Operating at High Speed near a Free Surface, Hydronautics, Inc. Technical Report 119-3, December 1, 1961.

[3] Lin, J. D. A Free Streamline Theory of Flows about a Flat Plate with a Flap at Zero Cavitation Number, Hydronautics, Inc. Technical Report 119-3, December 1, 1961.

[4] Wetzel, J. M. and Schiebe, F. R. Lift and Drag on Surface-Piercing Dihedral Hydrofoils in Regular Waves, University of Minnesota, St. Anthony Falls Hydraulic Laboratory Project Report No. 64, September 1960.

[5] Wetzel, J. M. and Maxwell, W. H. C. Tandem Interference Effects of Flat, Noncavitating Hydrofoils, University of Minnesota, St. Anthony Falls Hydraulic Laboratory Project Report No. 61, May 1962.

[6] Jones, C. E. Jr. Flapped Hydrofoils in Smooth Water Subcavitating Flow, General Dynamics/Convair Report ZH-153, November 1961.

[7] Schiebe, F. R. and Wetzel, J. M. Ventilated Cavities on Submerged Three-Dimensional Hydrofoils, University of Minnesota, St. Anthony Falls Hydraulic Laboratory Technical Paper No. 36, Series B, December 1961.

[8] Silberman, E. and Song, C. S. "Instability of Ventilated Cavities", Journal of Ship Research, Vol. 5, No. 1, June 1961.

[9] Song, C. S. "Pulsation of Ventilated Cavities", Journal of Ship Research, Vol. 5, No. 4, March 1962.

[10] Killen, John M. The Sonic Surface-Wave Transducer, University of Minnesota, St. Anthony Falls Hydraulic Laboratory Technical Paper No. 23, Series B, July 1959.

[11] Johnson, Virgil E. Jr. Theoretical and Experimental Investigation of Supercavitating Hydrofoils Operating near the Free Water Surface, National Aeronautics and Space Administration, Technical Report R-93, 1961.

[12] Wu, T. Yao-Tsu "A Free Streamline Theory for Two-Dimensional Fully Cavitated Hydrofoils", Journal of Mathematics and Physics, Vol. XXXV, No. 3, October 1956.

F I G U R E S

(1 through 13)

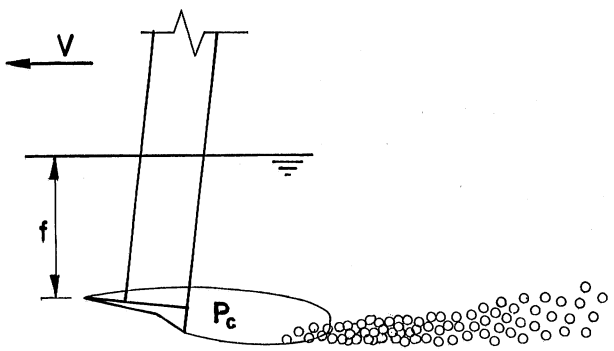

$$\sigma = \frac{P_o - P_c}{\frac{1}{2}\rho V^2}$$

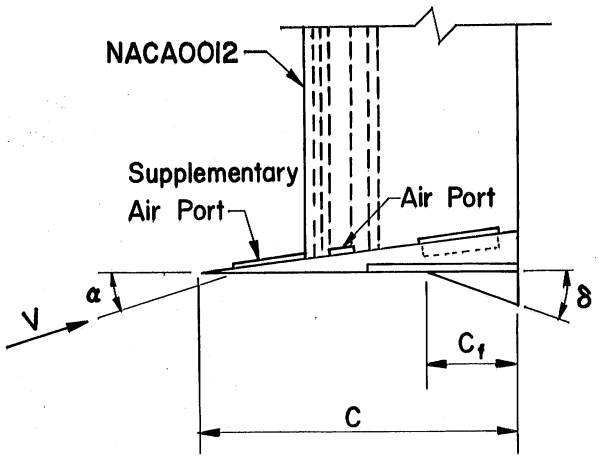

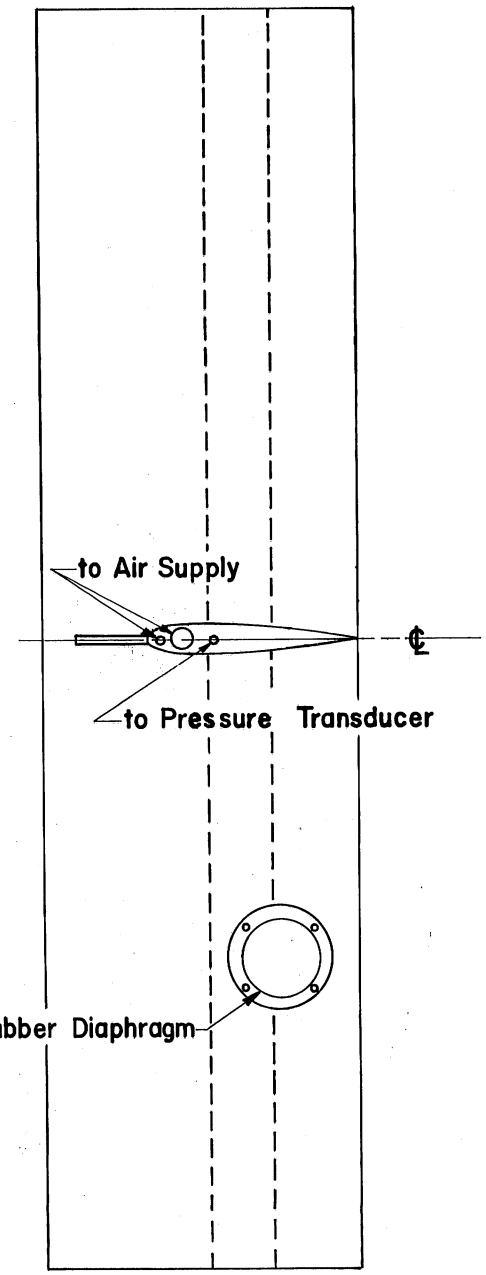

3" x 12" Wedge Flat Plate			
α	f/c	c_f/c	δ tested at 16 fps
7	0.5	0.25	16
7	1.0	0.25	16
7	2.0	0.25	16
8	1.0	0.25	0, 4, 8, 12, 16, 20
8	1.0	0.50	0, 8, 16
10	1.0	0.25	0, 4, 8, 12, 16, 20
10	1.0	0.50	0, 8, 16
14	0.5	0.25	16
14	1.0	0.25	0,4,6,8,12,16,20
14	1.0	0.50	0, 8, 16
18	0.5	0.25	16
18	1.0	0.25	0, 4, 6, 8, 12, 16

3" x 18" Wedge Flat Plate			
α	f/c	c_f/c	δ tested at 16 fps
8	1.0	0.25	0, 8, 16
10	1.0	0.25	0, 8, 16
10	2.0	0.25	0
14	1.0	0.25	0, 8, 16
14	2.0	0.25	0
18	1.0	0.25	0
18	2.0	0.25	0

TABLE I

Fig. 1 - Definition Sketch and Table I

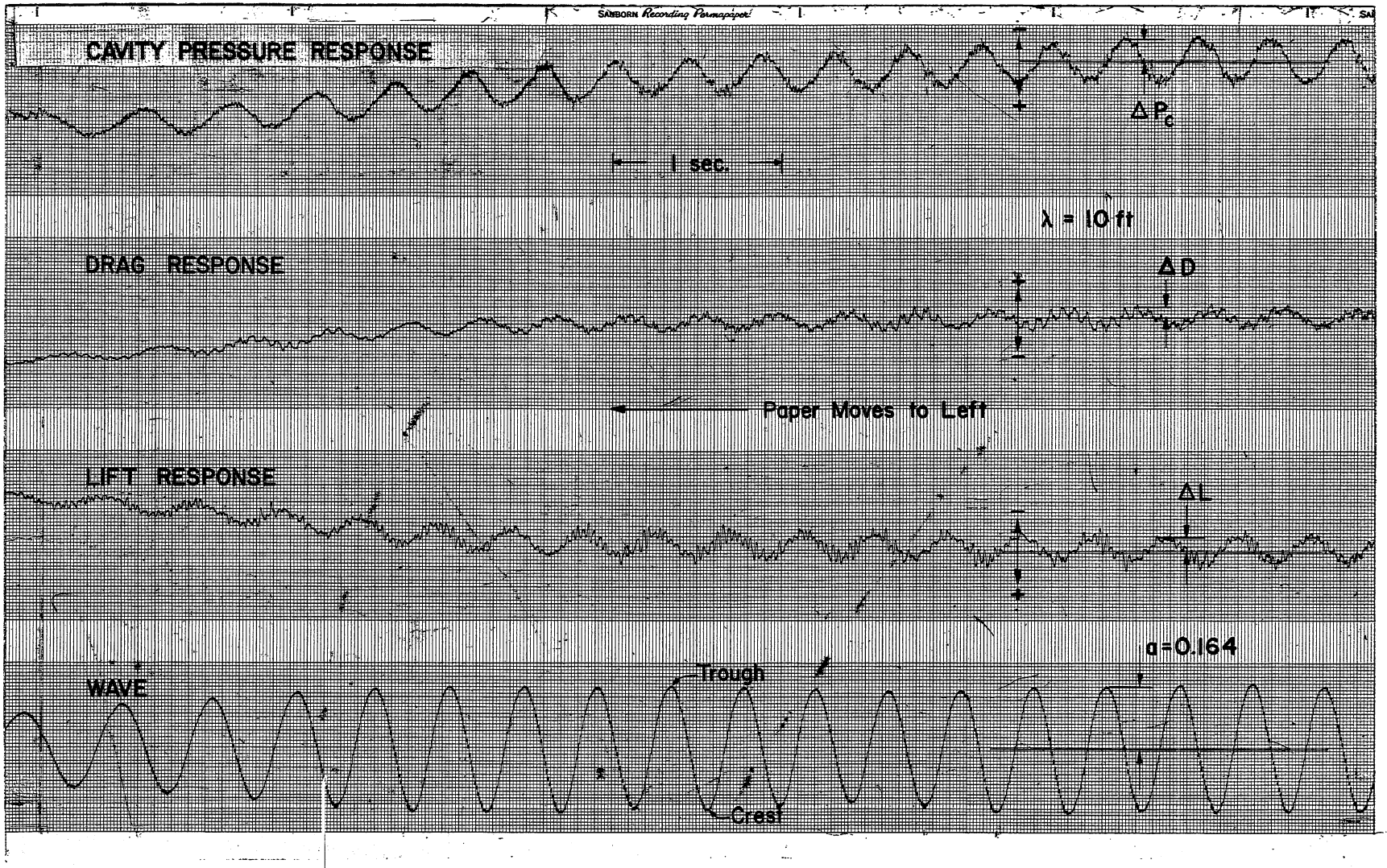

Fig. 2 - Typical Experimental Record for Ventilated Foil moving through Head Seas, AR = 4, V = 16 fps, f = lc, $c_f/c = 0.25$, $\alpha = 10^\circ$, $\delta = 16^\circ$

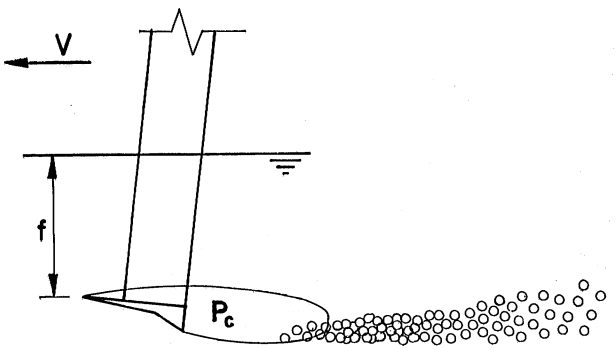

$$\sigma = \frac{P_o - P_c}{\frac{1}{2}\rho V^2}$$

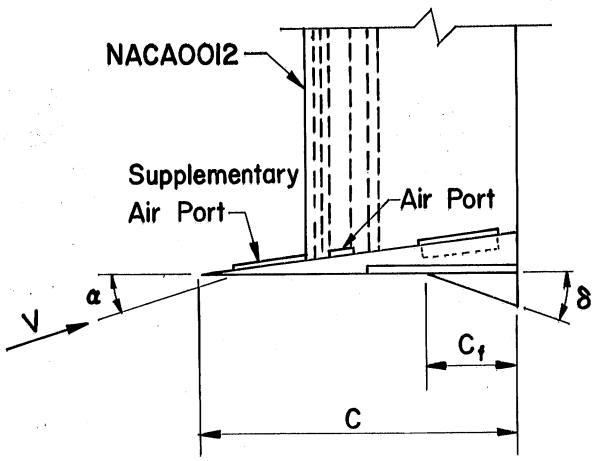

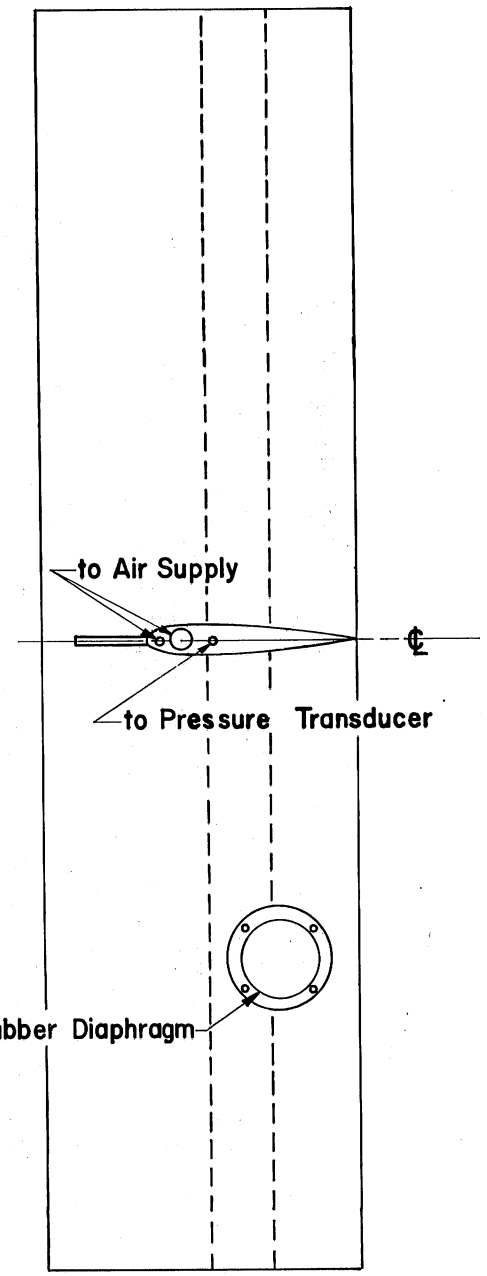

3" x 12" Wedge Flat Plate			
α	f/c	c_f/c	δ tested at 16 fps
7	0.5	0.25	16
7	1.0	0.25	16
7	2.0	0.25	16
8	1.0	0.25	0, 4, 8, 12, 16, 20
8	1.0	0.50	0, 8, 16
10	1.0	0.25	0, 4, 8, 12, 16, 20
10	1.0	0.50	0, 8, 16
14	0.5	0.25	16
14	1.0	0.25	0,4,6,8,12,16,20
14	1.0	0.50	0, 8, 16
18	0.5	0.25	16
18	1.0	0.25	0, 4, 6, 8, 12, 16

3" x 18" Wedge Flat Plate			
α	f/c	c_f/c	δ tested at 16 fps
8	1.0	0.25	0, 8, 16
10	1.0	0.25	0, 8, 16
10	2.0	0.25	0
14	1.0	0.25	0, 8, 16
14	2.0	0.25	0
18	1.0	0.25	0
18	2.0	0.25	0

TABLE I

Fig. 1 - Definition Sketch and Table I

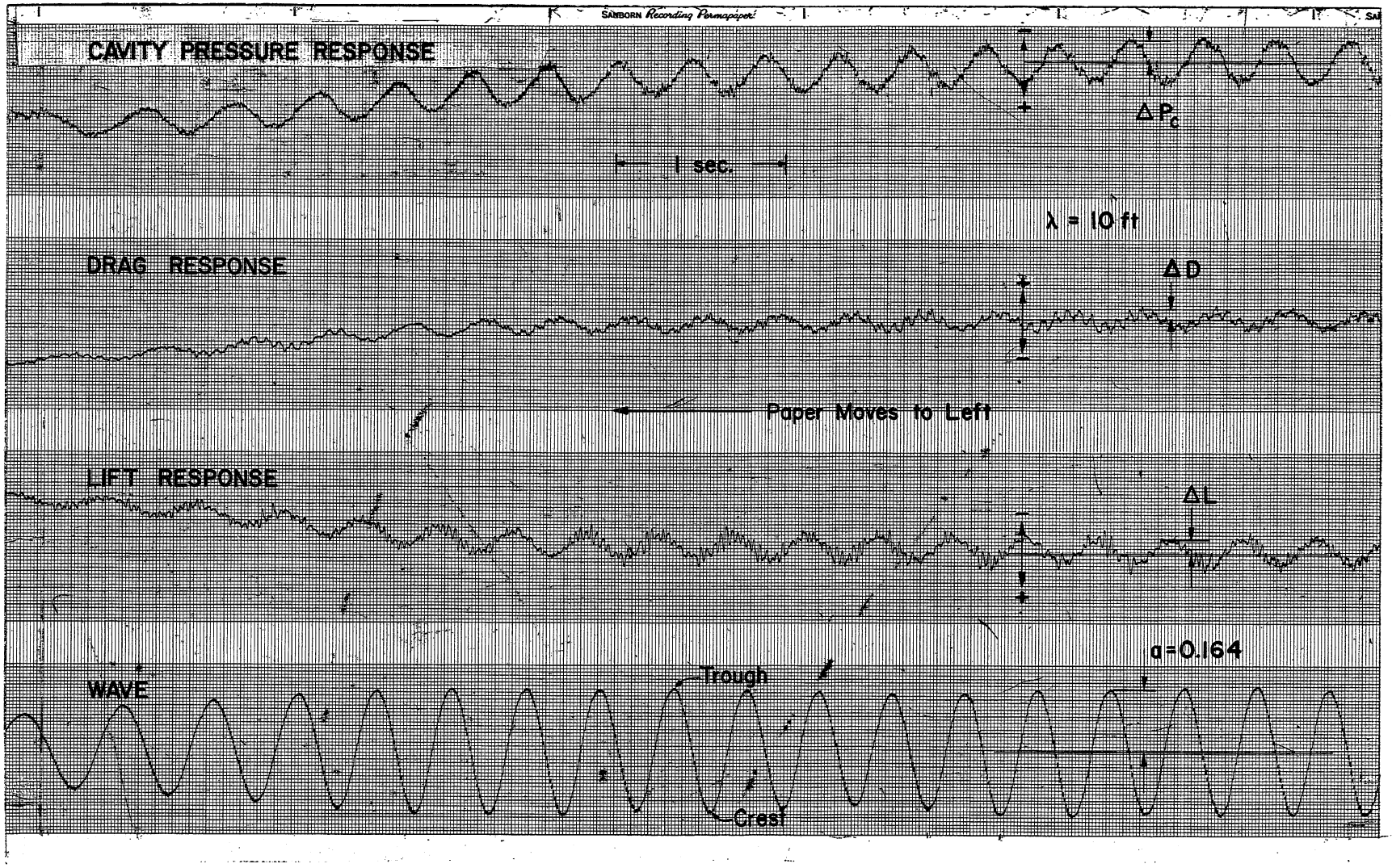

Fig. 2 - Typical Experimental Record for Ventilated Foil moving through Head Seas, AR = 4, V = 16 fps, f = lc, $c_f/c = 0.25$, $\alpha = 10^\circ$, $\delta = 16^\circ$

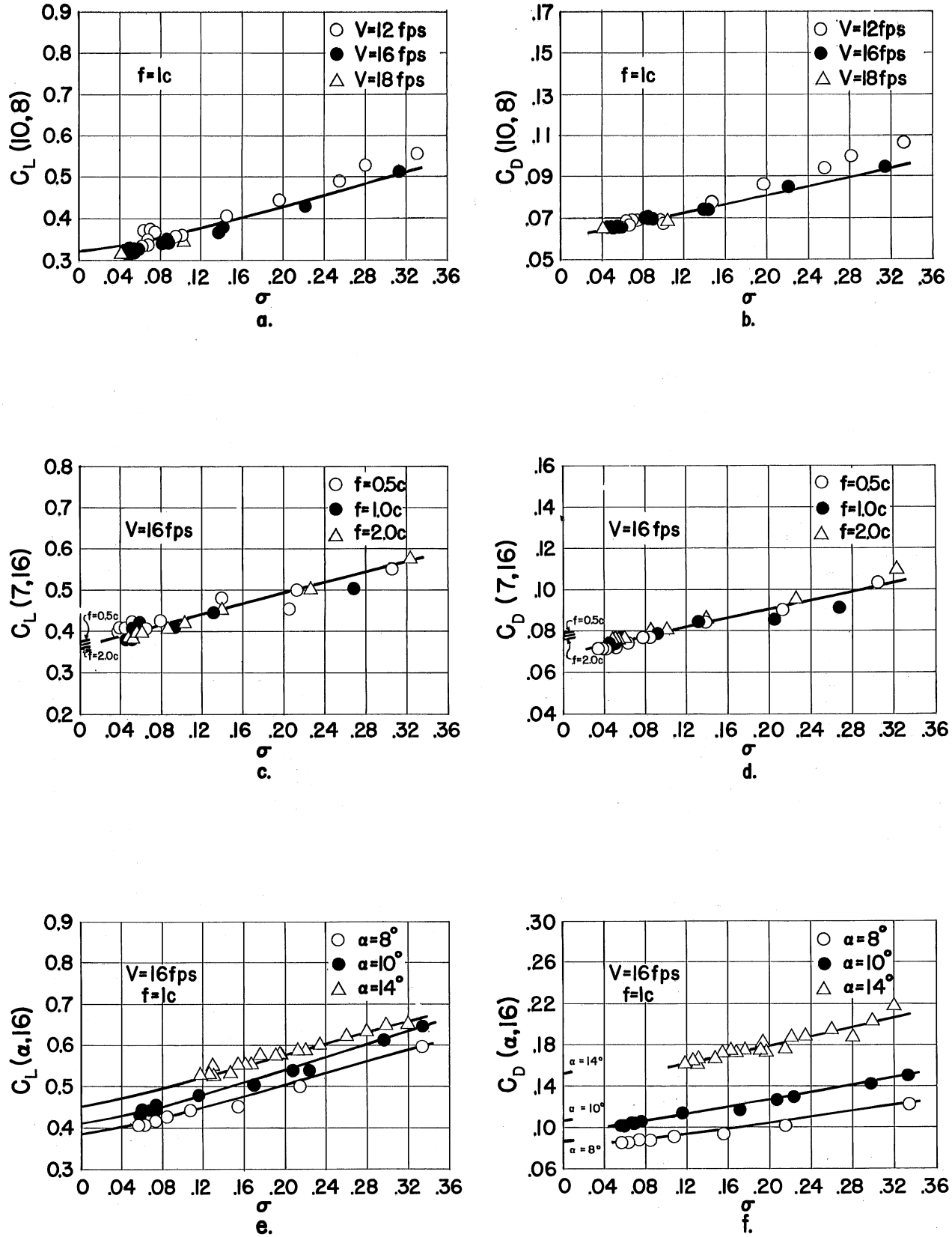

Fig. 3 - Effect of Velocity, Submergence, and Angle of Attack on Force Coefficients in Smooth Water, AR = 4, $c_f/c = 0.25$

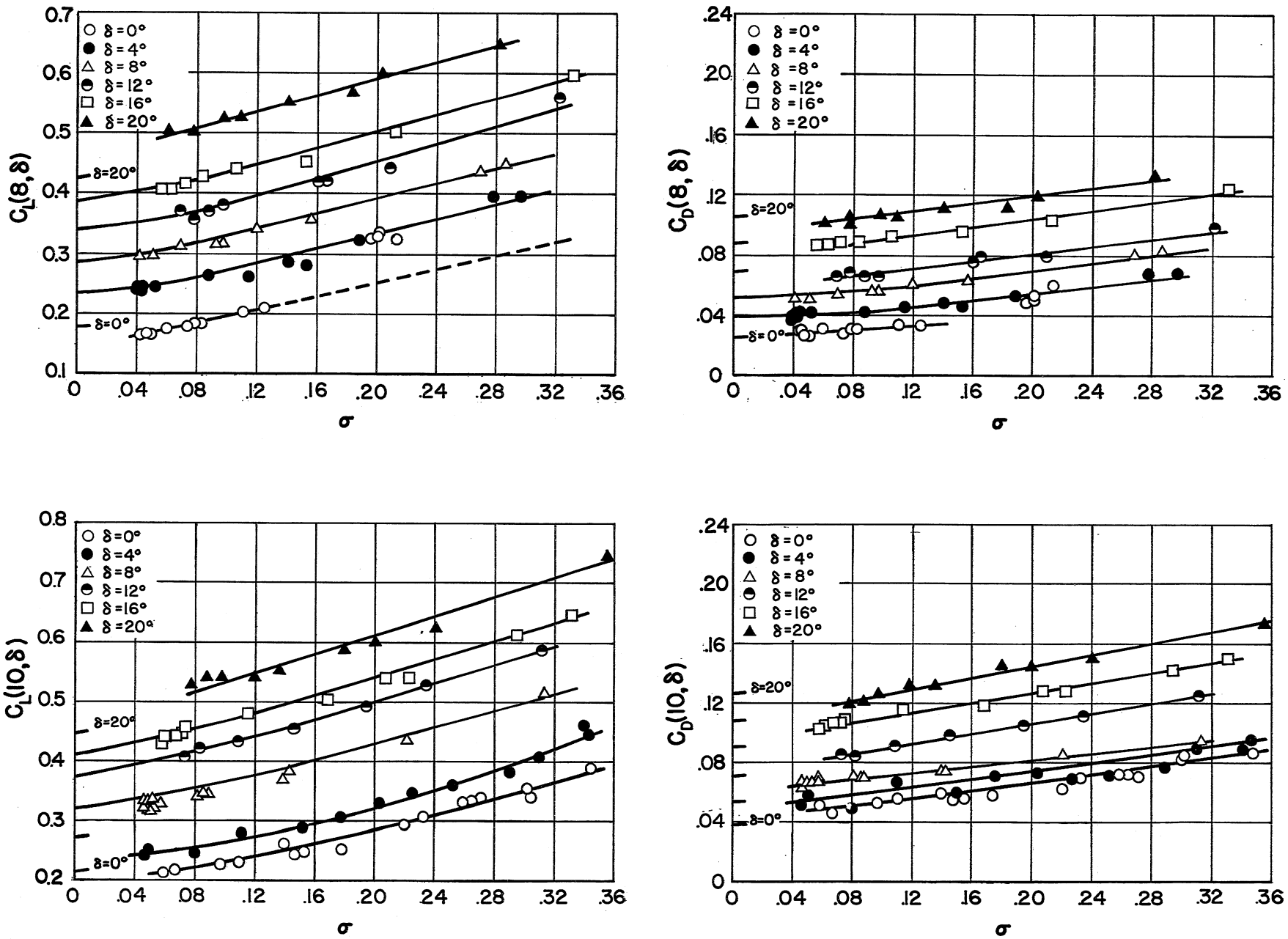

Fig. 4 - Force Coefficients for Flapped Foil in Smooth Water, AR = 4, V = 16 fps, f = 1c, $^{c}f/c = 0.25$

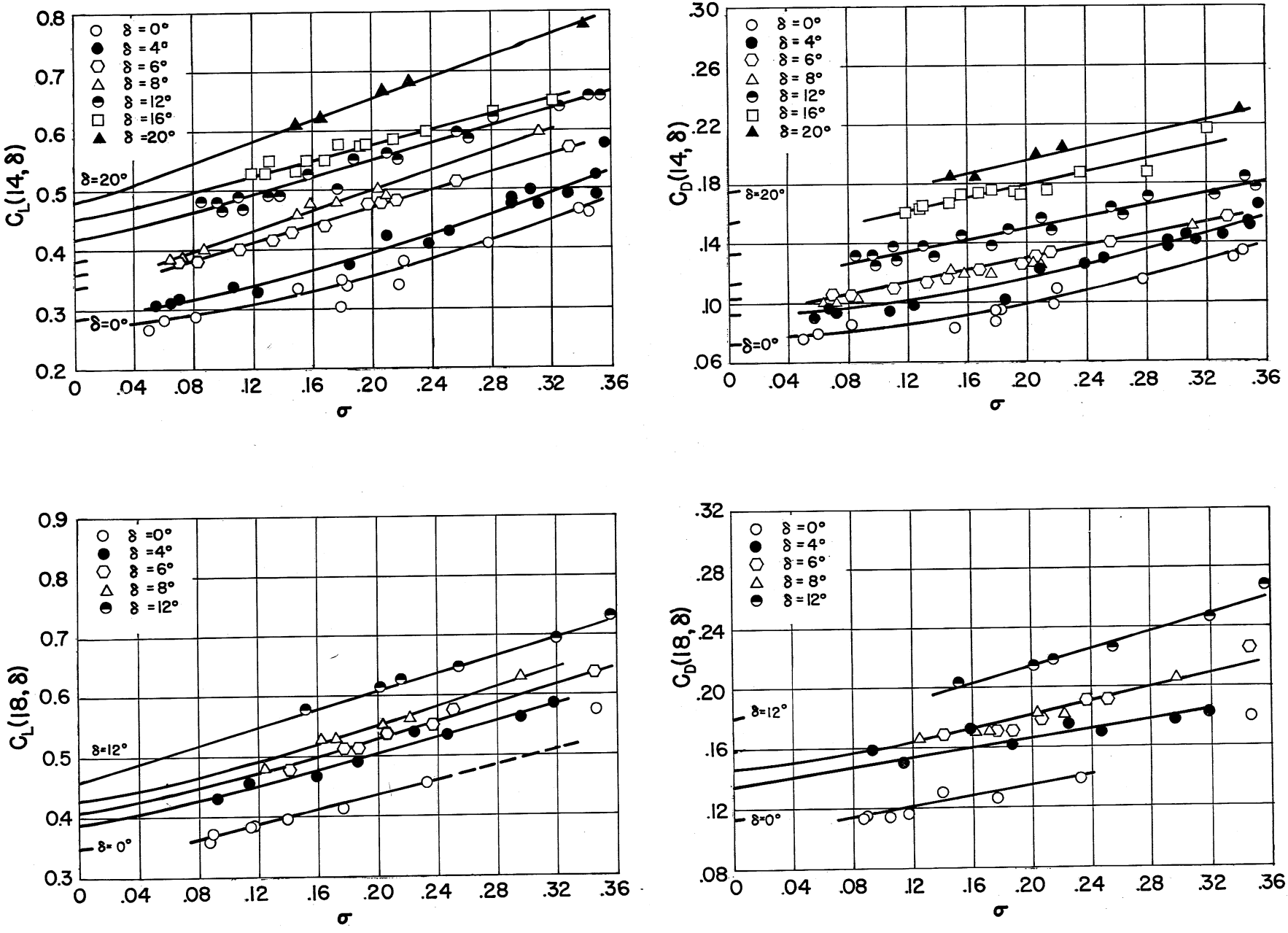

Fig. 4 - Force Coefficients for Flapped Foil in Smooth Water, AR = 4, V = 16 fps, f = 1c, $^{c}f/c = 0.25$ (cont'd)

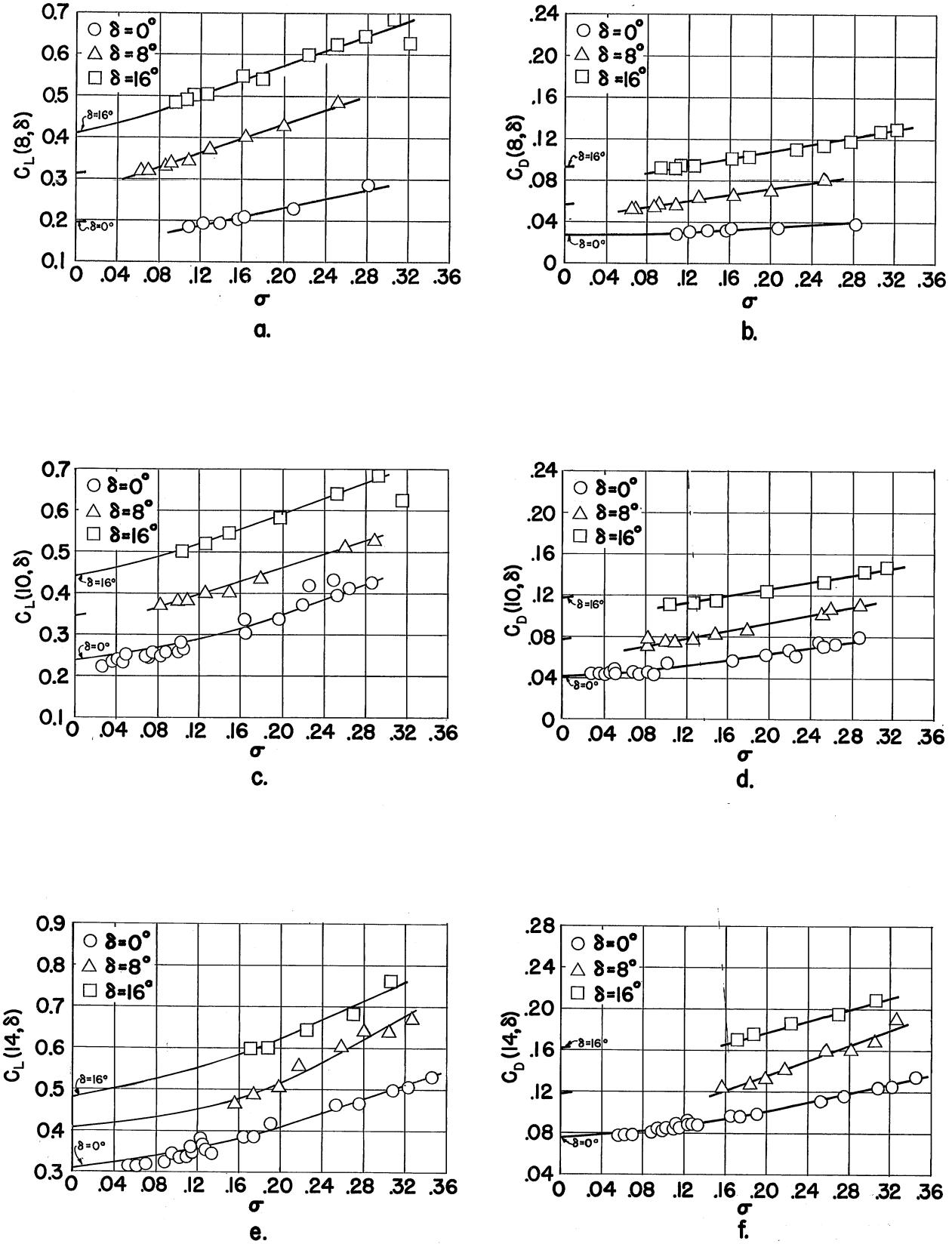

Fig. 5 - Force Coefficients for Flapped Foil in Smooth Water, AR = 6, V = 16 fps, f = lc, $c_f/c = 0.25$

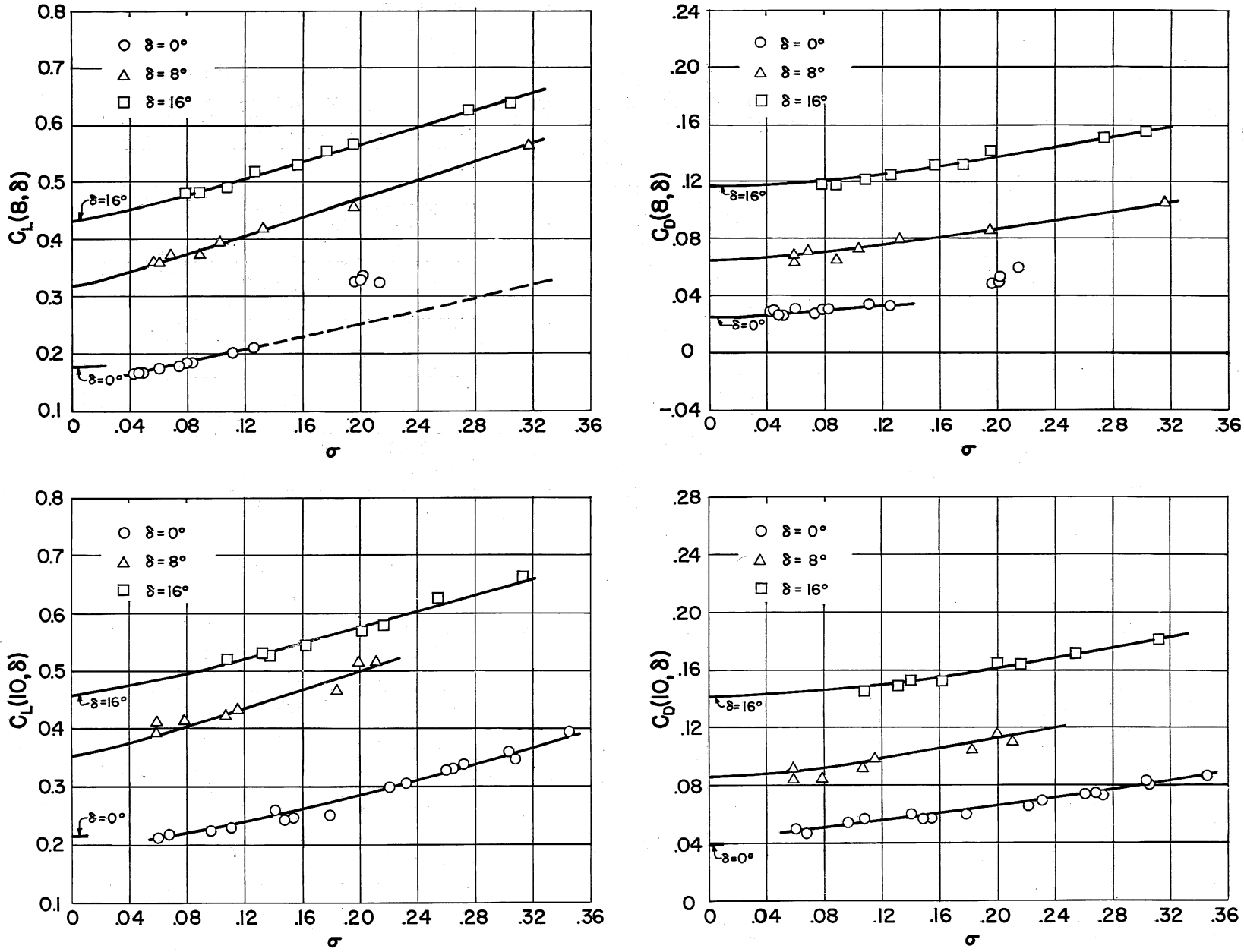

Fig. 6 - Force Coefficients for Flapped Foil in Smooth Water, AR = 4, V = 16 fps, f = 1c, $^{c}f/c = 0.5$

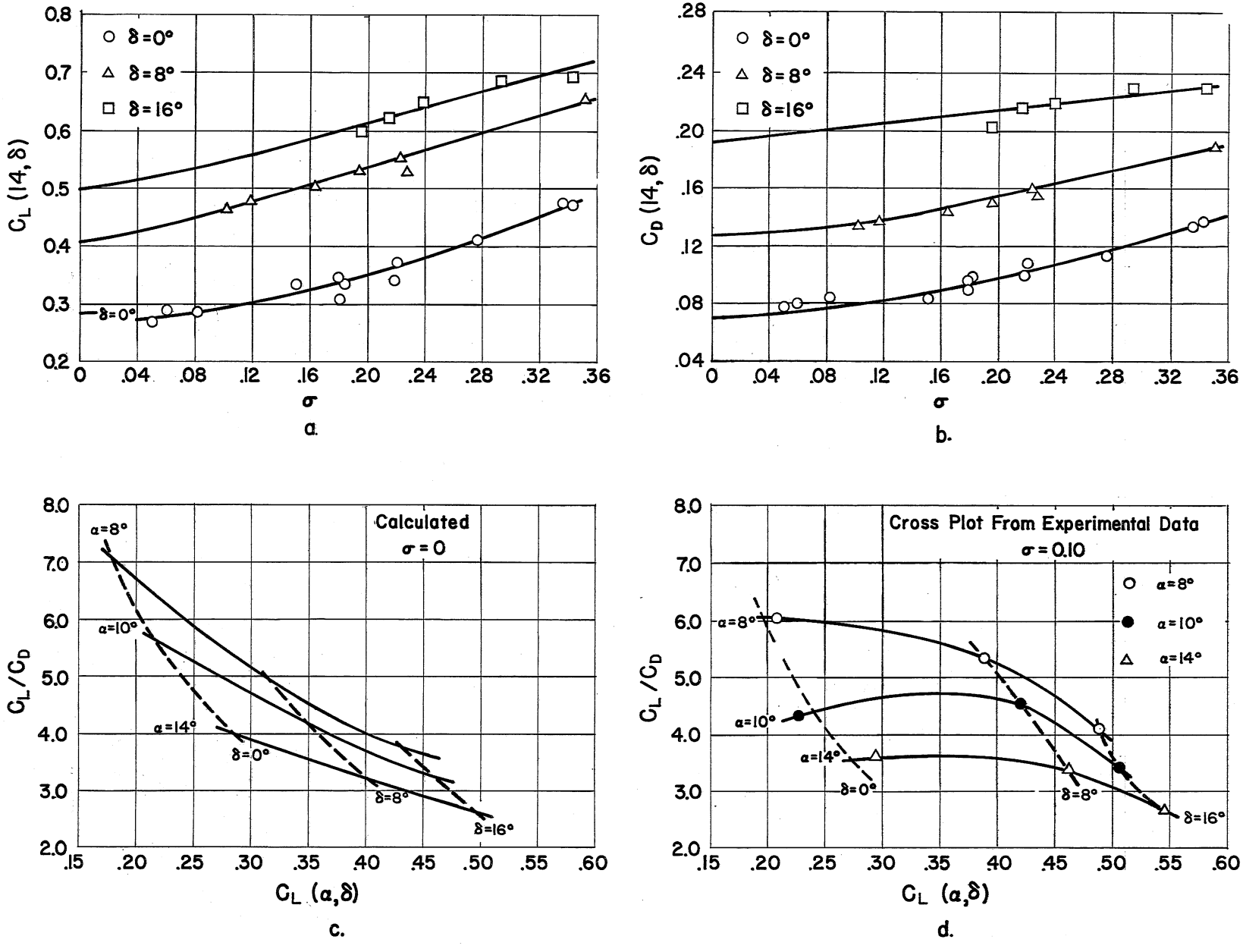

Fig. 7 - Force Coefficients and Lift-Drag Ratios in Smooth Water, AR = 4, V = 16 fps, f = 1c, $^{c}f/c = 0.5$

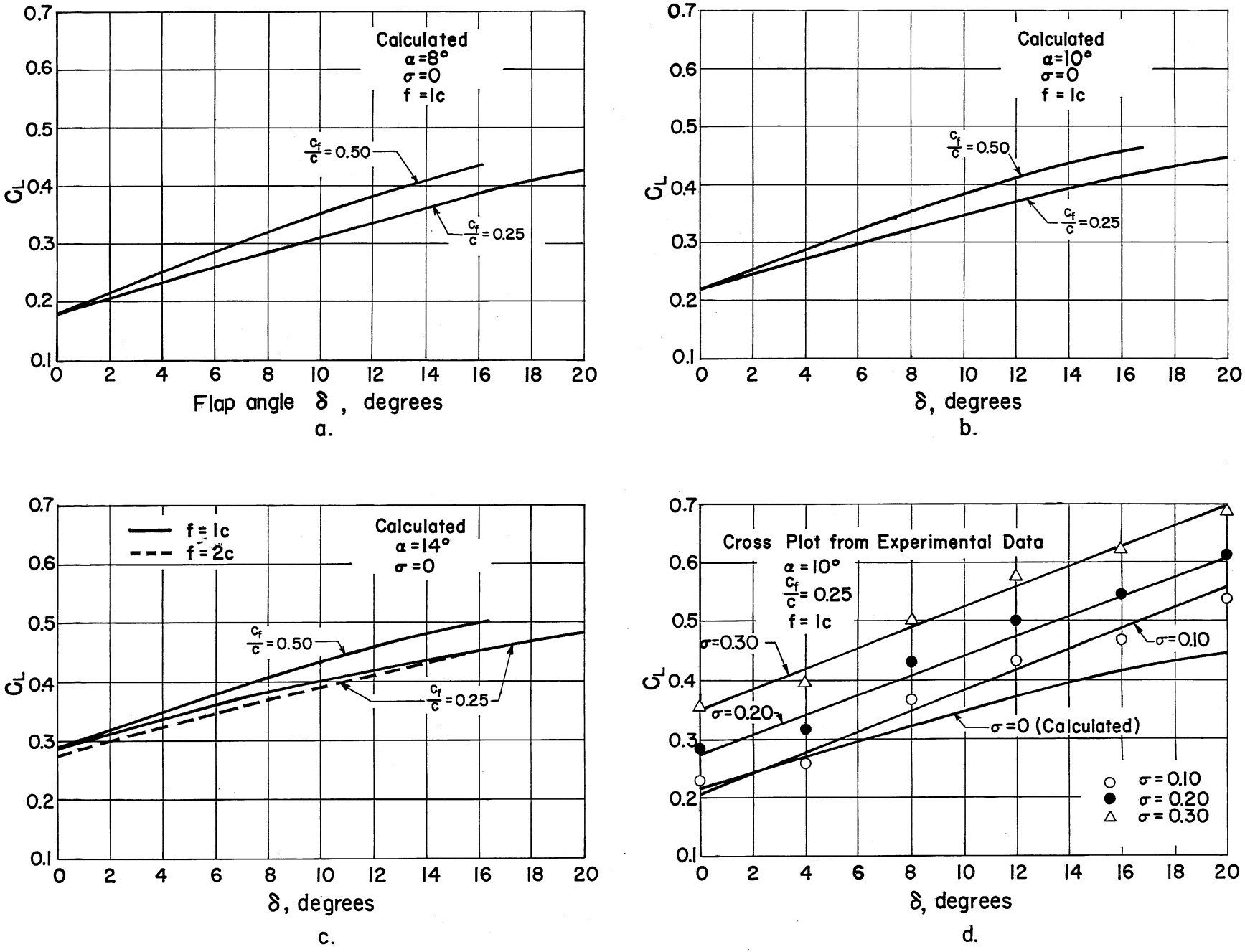

Fig. 8 - Effectiveness of Flap for Two Flap-Chord Ratios in Smooth Water, AR = 4, V = 16 fps

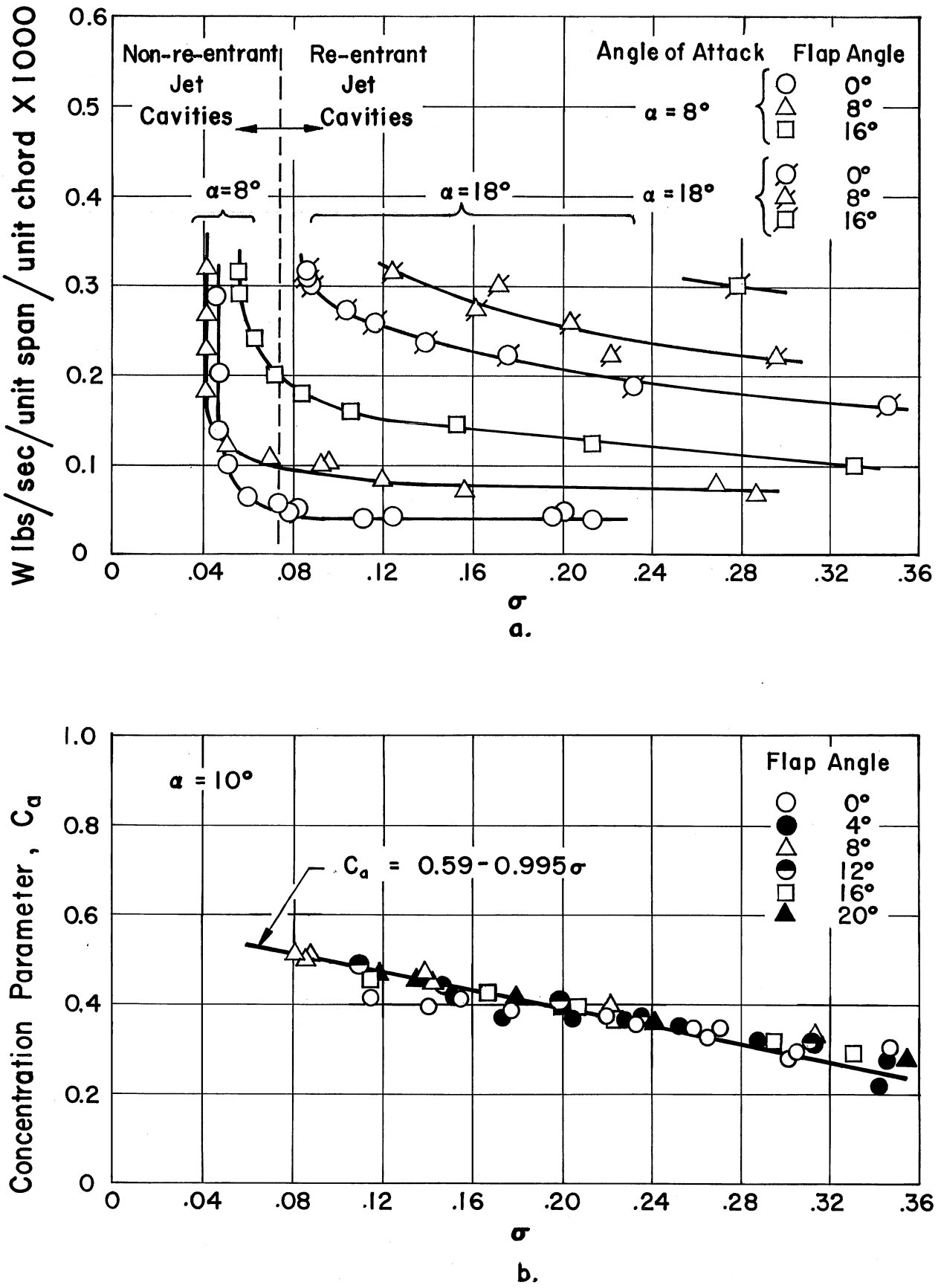

Fig. 9 - Typical Air-Entrainment Data in Smooth Water, AR = 4, V = 16 fps, f = 1c, $^{c}f/c = 0.25$

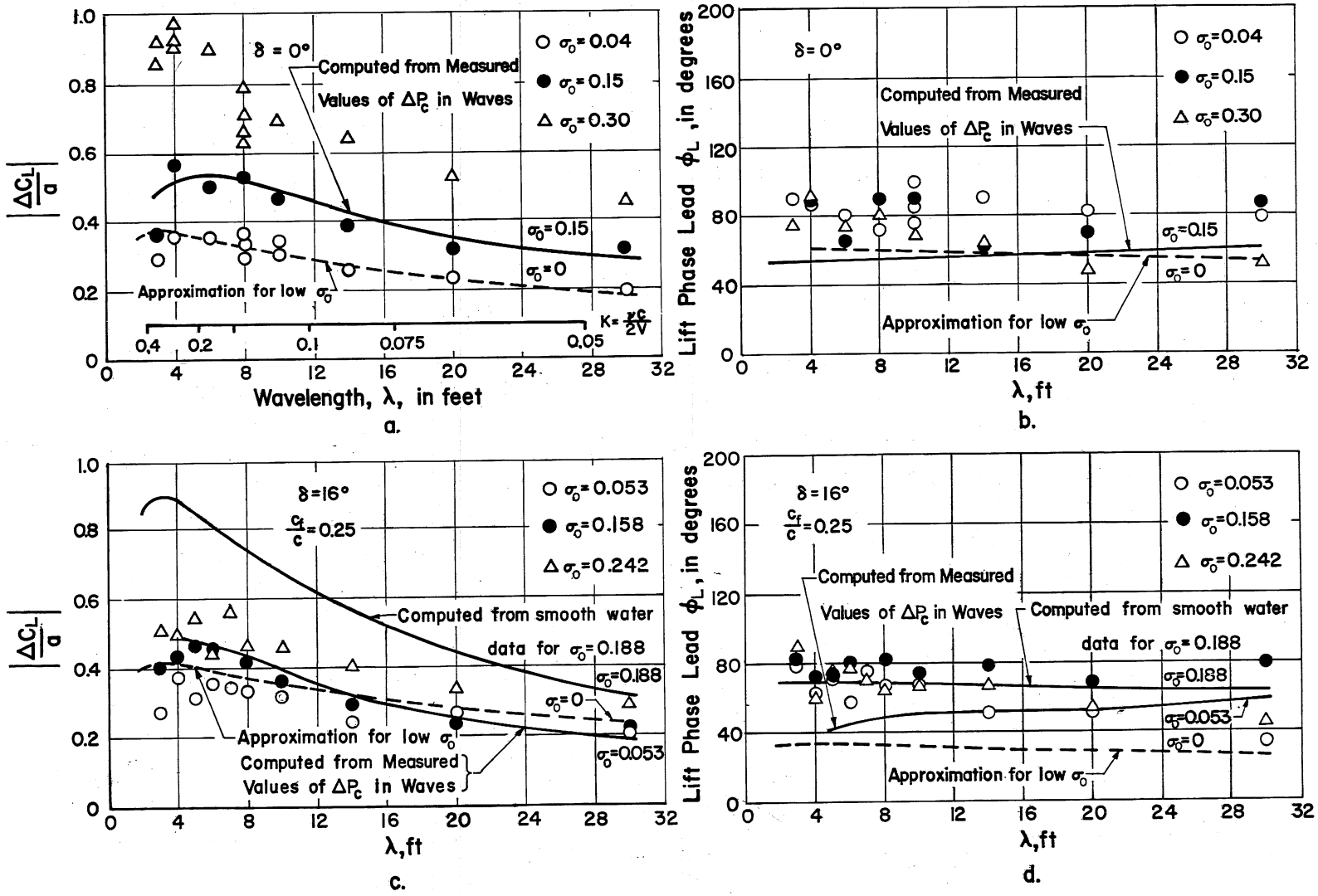

Fig. 10 - Amplitude and Phase for Oscillatory Lift Response for Foil in Head Seas, AR = 4, V = 16 fps, f = 1c, $\alpha = 10^{\circ}$, a = 0.15 ft

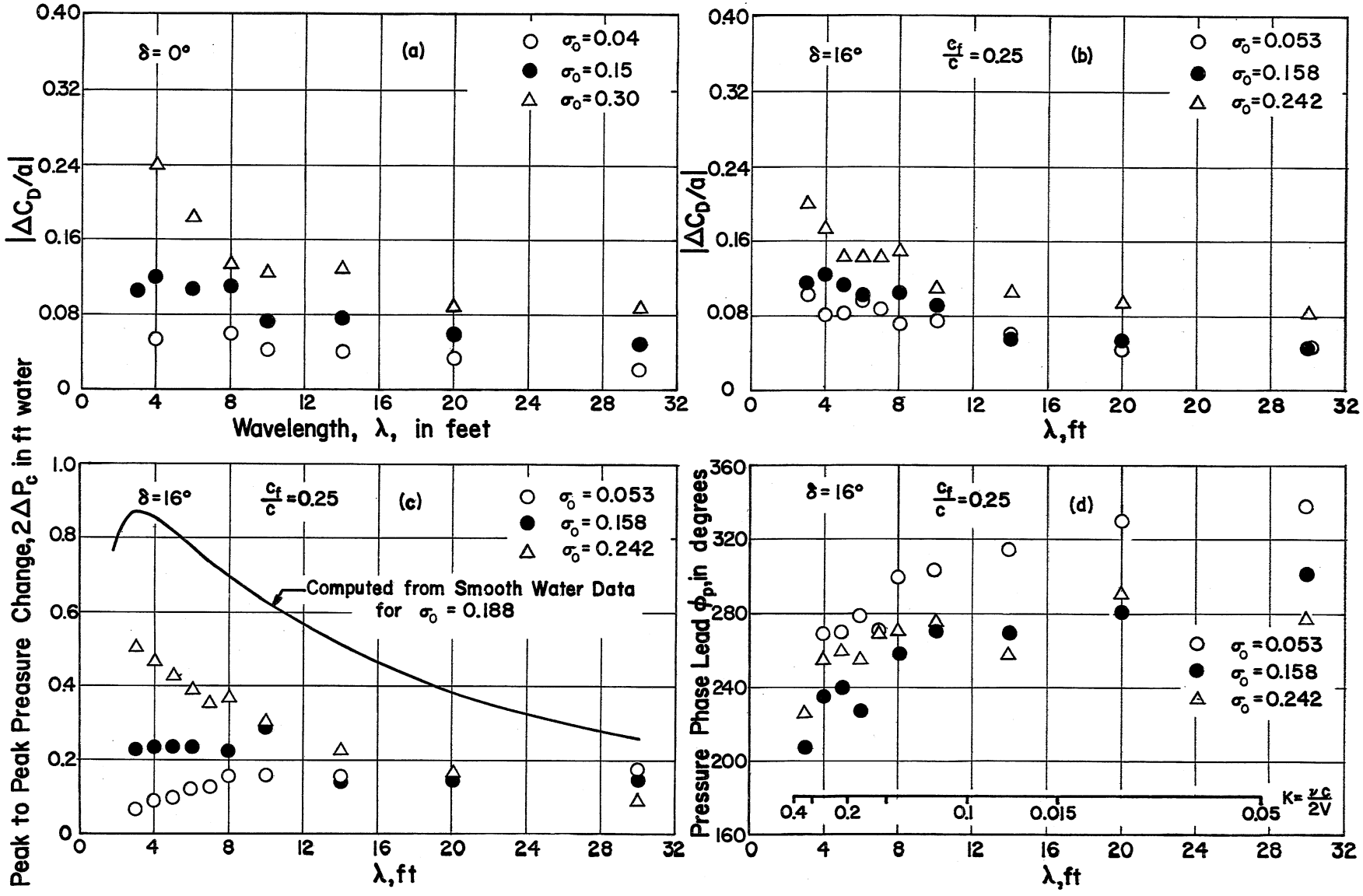

Fig. 11 - Oscillatory Drag and Cavity Pressure Data for Foil in Head Seas, AR = 4, V = 16 fps, f = 1c, $\alpha = 10^{\circ}$, a = 0.15 ft

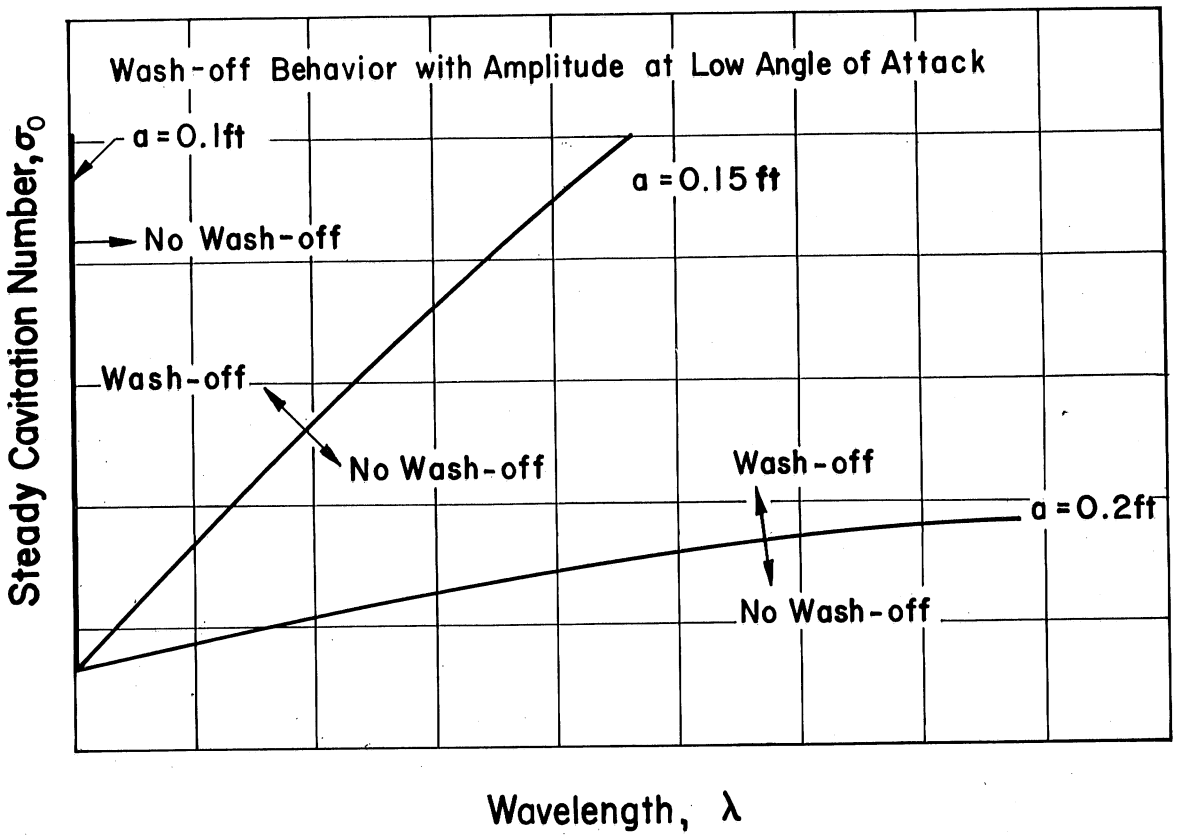

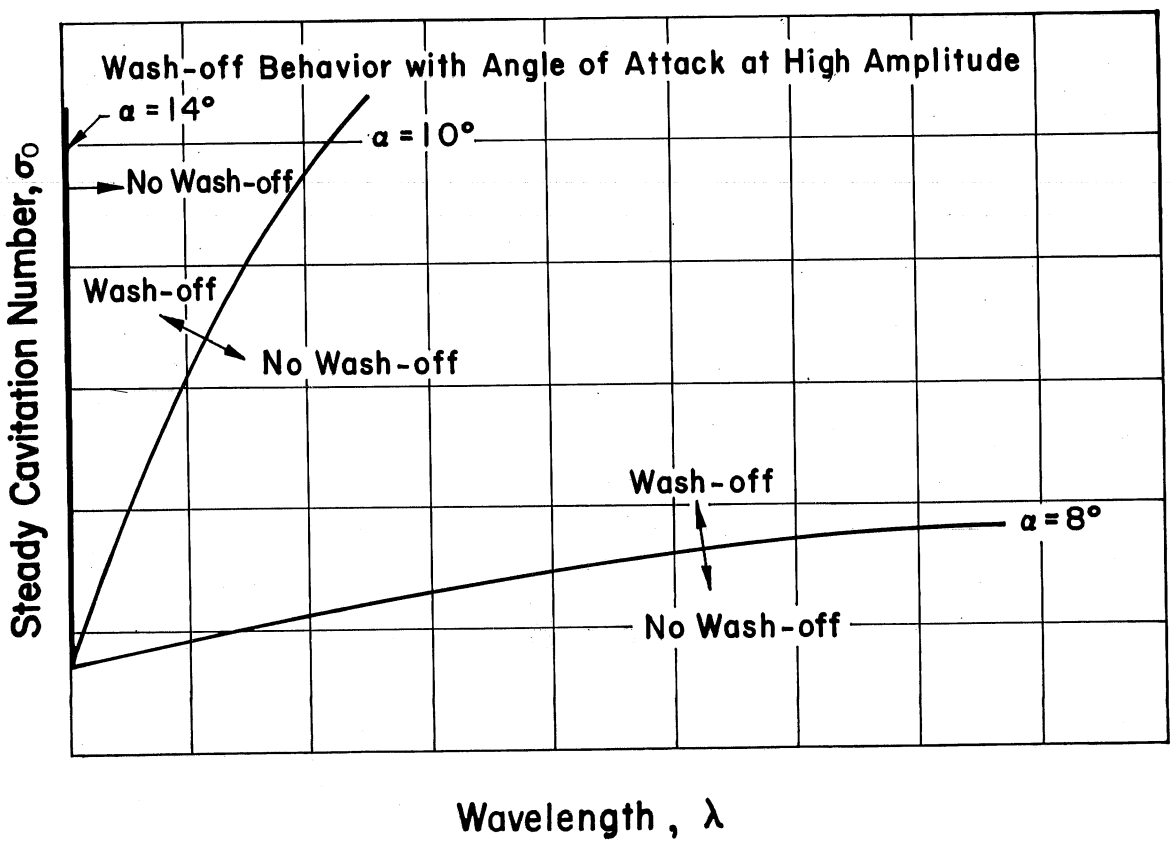

Fig. 12 - Trend of Cavity Wash-Off Behavior with Wave Amplitude and Angle of Attack

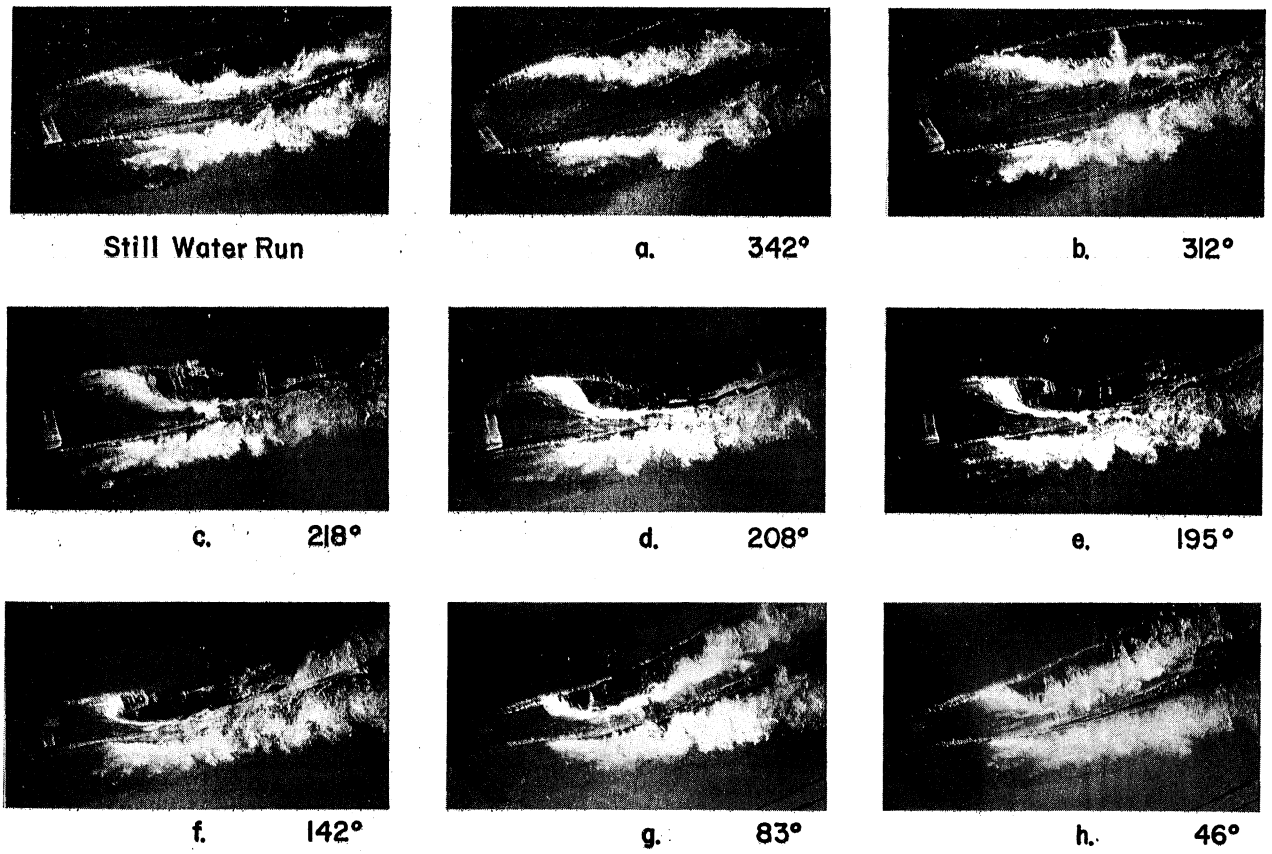

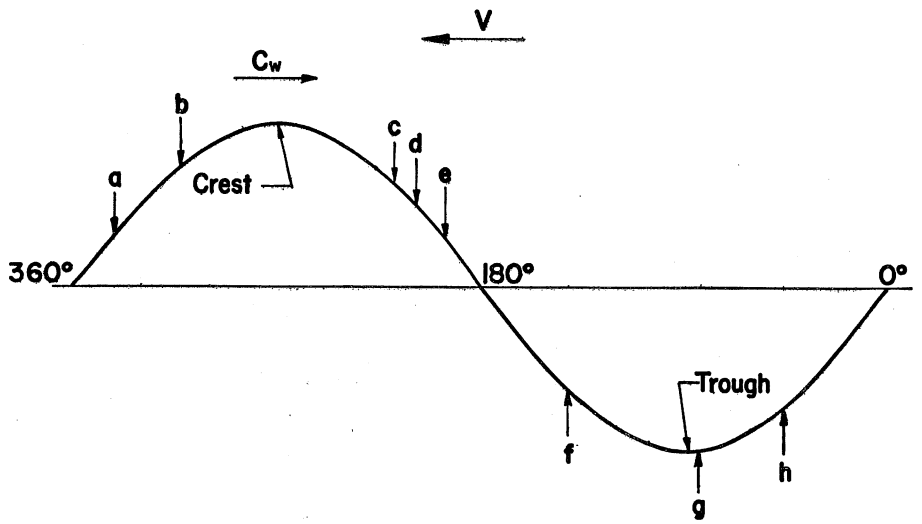

Fig. 13 - Typical Photographs of Ventilated Foil without Flap Moving Through Head Seas, AR = 4, V = 16 fps, f = 1c, $\alpha = 14^{\circ}$, $\lambda = 10$ ft, a = 0.1 ft, $\sigma_o = 0.14$

A P P E N D I X A

Modification of Theory for Two-Dimensional Foils in an Infinite Fluid

APPENDIX A

Modification of Theory for Two-Dimensional Foils in an Infinite Fluid

A. Correction for Finite Depth (Lin [3])

All existing theory for flapped supercavitating hydrofoils has been developed for two-dimensional foils operating at $\sigma = 0$. In order to compare theory with experimental data, attempts were made to modify the two-dimensional theory by a method previously used by Johnson [11]. Lin [3] has developed a non-linear theory for a foil in an infinite fluid, but the complicated integrals required numerical integration by a digital computer. To increase the usefulness of his theory, Lin then adopted a method similar to that used by Johnson to calculate the lift force, and also modified the results to include effects of finite depth. In this section, the preceding method will be further modified to include effects of finite span. It will first be of interest to summarize the procedure used by Lin to simplify his theory.

Rayleigh's formula based on non-linear theory for a two-dimensional flat plate and $\sigma = 0$ was modified to include a foil with flaps operating at a finite submergence by using an effective angle of incidence α_e, thus

$$C_L(\alpha,\delta) = \frac{2\pi \sin \alpha_e \cos \alpha_{eq}}{4 + \pi \sin \alpha_e} \qquad \text{(A-1)}$$

where α_{eq} = angle of incidence of an equivalent flat plate

$\alpha_e = \alpha_{eq} + \alpha_c$

α_c = angle of incidence due to camber

Both the angles α_{eq} and α_c were calculated from linearized theory [2].

Then, $C_L(\alpha,\delta) = C_L(\alpha,0) + C_L(0,\delta)$

and $C_L(0,\delta) = \frac{\pi}{2}\alpha_e' = \frac{\pi}{2}(\alpha' + \alpha_c')$

where $'$ refers to part related to $C_L(0,\delta)$

Here the effect of the angle of attack has been broken into two parts; the rotation of the foil reference line due to flap deflection, α',

and the angle due to camber caused by flap deflection, α_c. These angles have been calculated by linearized theory, and

$$\alpha' = \delta\left(\frac{\pi - \theta_h}{\pi}\right)$$

$$\alpha_c' = \frac{2\delta}{\pi} \sin\theta_h\left(1 - \frac{1}{2}\cos\theta_h\right)$$

where $\theta_h = \arccos\left(1 - 2\sqrt{1 - \frac{c_f}{c}}\right)$

Thus, $\alpha_e = \alpha + \alpha_e' = \alpha + \alpha' + \alpha_c'$

and $\alpha_{eq} = \alpha + \alpha'$

Substitution of the equations for α_e and α_{eq} into Eq. (A-1) gave results for the lift coefficient that agreed favorably with those calculated from exact theory by Lin.

To include effects of finite depth of submersion, Lin then proceeded to modify Green's formula to include flapped foils. Thus, from the linearized solution, α_e' could be found from

$$\frac{\alpha_e'}{\delta} = C_L(0,\delta)\Big|_{\frac{c_f}{c}} \Big/ C_L(0,\delta)\Big|_{\frac{c_f}{c}=1} \qquad \text{(A-3)}$$

$C_L(0,\delta)$ can be determined from Eq. (17) of Ref. [2],

$$C_L(0,\delta) = 2A\delta\left(\frac{\pi}{2} - \arcsin\sqrt{\bar{d}}\right)\left(1 - 2\sqrt{a(1+a)}\right) + \sqrt{\bar{d}}\sqrt{1-\bar{d}}$$

$$+ 2a\left(\arctan\sqrt{\frac{a}{\bar{d}}} - \arctan\frac{\sqrt{a\bar{d}}}{1 + \sqrt{(1-\bar{d})(1+a)}}\right) \qquad \text{(A-4)}$$

Also, for any angle θ, Eq. (18) of the same reference gives

$$C_L(0,\theta)\Big|_{\frac{c_f}{c}=1} = C_L(\theta,0) = \theta\pi A[1+a]\left(1 - \sqrt{\frac{a}{1+a}}\right)^2 \qquad \text{(A-5)}$$

where $a = \frac{f/c}{A\pi}$

$$\frac{1}{A} = 1 - a \ln\left(\frac{1}{a} + 1\right)$$

Auslaender defined $\bar{d}$ as the non-dimensional distance in the airfoil plane, corresponding to the non-dimensional distance, d, between the leading edge of the hydrofoil and the flap hinge in the hydrofoil plane. Thus,

$$d = 1 - \frac{c_f}{c}$$

and $\bar{d}$ can be found from the mapping function or transformation of the hydrofoil coordinates to airfoil coordinates,

$$\frac{d}{aA} = \frac{\bar{d}}{a} - \ln\left(1 + \frac{\bar{d}}{a}\right) \qquad \text{(A-6)}$$

It can thus be seen that $\bar{d}$ is a function of flap to chord ratio, $\frac{c_f}{c}$, and depth to chord ratio, f/c in the hydrofoil plane.

The rotation of the hydrofoil reference line, α', is

$$\alpha' = \frac{\delta}{\pi} \arccos\left(2\bar{d} - 1\right) \qquad \text{(A-7)}$$

It is therefore possible to calculate α_e and α_{eq}. The lift curve slope, m_e, can be taken from Fig. 2 of Ref. [11]. The modified lift coefficient was then written

$$C_L(\alpha,\delta) = m_e \alpha_e \frac{\cos \alpha_{eq}}{\cos \alpha_e} \qquad \text{(A-8)}$$

B. Correction for Finite Aspect Ratio

Following the method of Johnson, the assumption was made that the two-dimensional lift coefficient should be modified due to effects of the trailing vorticity. This resulted in the same effect as that for a fully wetted hydrofoil. Thus, the lift coefficient for a rectangular planform reduces to

$$C_{L_1} = \frac{AR}{1 + AR} m(\alpha_e - \alpha_i) \frac{\cos \alpha_{eq}}{\cos(\alpha_e - \alpha_i)} \qquad (A\text{-}9)$$

where AR = aspect ratio

m = lift curve slope

$$\alpha_i = \frac{C_{L_1}}{\pi AR} (1 + \tau)$$

τ = planform correction

Another effect of aspect ratio considered by Johnson was the additional lift due to crossflow. For a flat plate, this effect was written as

$$C_{L_C} = \frac{1}{1 + AR} 0.88 \sin^2(\alpha_{eq} + \alpha_c') \cos(\alpha + \alpha') \qquad (A\text{-}10)$$

In terms of the previously defined quantities,

$$C_{L_c} = \frac{1}{1 + AR} 0.88 \sin^2(\alpha + \alpha' + \alpha_c') \cos(\alpha + \alpha') \qquad (A\text{-}11)$$

The total lift coefficient is thus the sum of the two equations (A-9) and (A-11), or

$$C_L = \frac{AR}{1 + AR} m(\alpha_e - \alpha_i) \frac{\cos \alpha_{eq}}{\cos(\alpha_e - \alpha_i)}$$

$$+ \frac{1}{1 + AR} 0.88 \sin^2(\alpha + \alpha' + \alpha_c') \cos(\alpha + \alpha') \qquad (A\text{-}12)$$

Johnson has shown that C_{L_c} is largest for large angles of attack, small aspect ratios, and large cambers. Therefore, since Eq. (A-10) is only an approximation for cambered foils, the error introduced by the crossflow coefficient will be greatest for the previously mentioned cases.

The computation for the total lift coefficient necessitates a trial and error procedure, as the induced angle, α_i, depends upon C_{L_1}. Furthermore, the planform correction τ is a function of the lift curve slope m, which cannot be determined until $\alpha_e - \alpha_i$ is known. It is thus necessary to assume a trial lift coefficient, C_{L_1}, and a planform correction factor, τ, from which α_i, α_e, and finally m can be found. The calculated value of C_{L_1} was compared with the assumed value, and the procedure

continued until the two values agreed. The convergence of the solution was quite rapid.

A P P E N D I X B

Theoretical Consideration of the Effect of Waves on Lift and Drag

APPENDIX B

Theoretical Consideration of the Effect of Waves on Lift and Drag

A. General Considerations and Assumptions of Steady Theory

The analysis will be carried out for a restrained hydrofoil without flaps moving through the sinusoidal wave train

$$\eta = a \sin \nu t \tag{B-1}$$

The resultant horizontal and vertical velocity components due to the orbital motion induced by the waves then are respectively,

$$\begin{aligned} u &= \mp a\omega \ell^{-kf} \sin \nu t \\ w &= \pm a\omega \ell^{-kf} \cos \nu t \end{aligned} \tag{B-2}$$

The upper sign refers to head seas and the lower sign to following seas.

Only first order variations are considered in the variation of C_L. Since $C_L = C_L(\alpha,\sigma)$, it is assumed that

$$\begin{aligned} C_L &= C_L(\alpha_o,\sigma_o) + \frac{\partial C_L}{\partial \alpha}\bigg|_{\substack{\alpha_o,\sigma_o}} \Delta\alpha + \frac{\partial C_L}{\partial \sigma}\bigg|_{\alpha_o,\sigma_o} \Delta\sigma \\ &= C_{L_o} + \frac{\partial C_L}{\partial \alpha}\bigg|_{o} \Delta\alpha + \frac{\partial C_L}{\partial \sigma}\bigg|_{o} \Delta\sigma \end{aligned} \tag{B-3}$$

Where $\Delta\alpha$ is the change in α due to the orbital velocity components and $\Delta\sigma$ is the change in σ due to the change in velocity, submergence and cavity pressure. Moreover, ignoring skin friction effects and the deviation of the resultant force vector from the normal, it is assumed that

$$C_D = C_L \tan \alpha_g \tag{B-4}$$

Then the total lift, measured perpendicular to the direction of motion, is written

$$L = \frac{\rho A}{2} [(V - u)^2 + w^2] [C_L \cos \Delta\alpha + C_D \sin \Delta\alpha] \tag{B-5}$$

Now, letting $\bar{u} = \frac{u}{V}$, $\bar{w} = \frac{w}{V}$, the following approximations are made:

$$\sin \Delta\alpha \backsimeq \Delta\alpha = \tan^{-1} \frac{w}{V - u} \backsimeq \bar{w}$$

and $\cos \Delta\alpha \backsimeq 1$ since $\Delta\alpha$, $\bar{u}$ and $\bar{w}$ are $\ll 1$

Hence, combining Eqs. (B-3), (B-4), and (B-5), the oscillatory lift coefficient for the foil is

$$C_{L_w} = \frac{L}{\frac{\rho}{2}AV^2} = [(1 - \bar{u})^2 + \bar{w}^2][C_{L_o} + \left.\frac{\partial C_L}{\partial \alpha}\right|_o \Delta\alpha$$

$$+ \left.\frac{\partial C_L}{\partial \sigma}\right|_o \Delta\sigma][1 + \Delta\alpha \tan (\alpha_g + \Delta\alpha)]$$

$$\backsimeq [1 - 2\bar{u} + \bar{w} \tan \alpha_g][C_{L_o} + \left.\frac{\partial C_L}{\partial \alpha}\right|_o \bar{w} + \left.\frac{\partial C_L}{\partial \sigma}\right|_o \Delta\sigma] \qquad \text{(B-6)}$$

B. Theory Based on Smooth Water Data

Experimentally the curve relating α and σ for a fixed air-flow rate was obtained in smooth water by varying α and measuring the corresponding σ. By computing the $\Delta\alpha$ corresponding to a given wave length, wave amplitude, and velocity, the $\Delta\sigma$ corresponding to this change in α about the mean angle, α_o, was obtained.

The relationship between $\Delta\alpha$ and $\Delta\sigma$ may be expressed for simplicity as

$$\Delta\sigma = R\Delta\alpha = R\bar{w} \qquad \text{(B-7)}$$

where R is assumed to be a function of α_o and σ_o only, and is obtained experimentally as described above. This then assumes that variations due to the changing horizontal velocity component and submergence may be neglected and that $\Delta\alpha$ and $\Delta\sigma$ are in phase. The limitations of the assumptions that $\Delta\sigma = R\Delta\alpha$ will be discussed in Section E. It will be shown there that for a precise analysis a different relationship between α and σ should be used for each value of λ and a.

Substituting Eq. (B-7) into Eq. (B-6)

$$C_{L_w} \overset{\frown}{=} [1 - 2\bar{u} + \bar{w} \tan \alpha_g][C_{L_o} + \bar{w} \left(\frac{\partial C_L}{\partial \alpha}\bigg|_o + R \frac{\partial C_L}{\partial \sigma}\bigg|_o\right)]$$

$$\overset{\frown}{=} C_{L_o} + \bar{w} \left(\frac{\partial C_L}{\partial \alpha}\bigg|_o + R \frac{\partial C_L}{\partial \sigma}\bigg|_o\right) - 2\bar{u} C_{L_o} + \bar{w} C_{L_o} \tan \alpha_g$$

The change in the lift coefficient is written as

$$\Delta C_{L_w} = C_{L_w} - C_{L_o} \overset{\frown}{=} \bar{w} \left(\frac{\partial C_L}{\partial \alpha}\bigg|_o + R \frac{\partial C_L}{\partial \sigma}\bigg|_o + C_{D_o}\right) - 2\bar{u} C_{L_o}$$

Therefore

$$\frac{\Delta C_{L_w}}{a} = \pm \frac{\omega \ell^{-kf}}{V} \cos \nu t \left(\frac{\partial C_L}{\partial \alpha}\bigg|_o + R \frac{\partial C_L}{\partial \sigma}\bigg|_o + C_{D_o}\right) \pm 2 \frac{\omega \ell^{-kf}}{V} C_{L_o} \sin \nu t$$

$$= \sqrt{A^2 + B^2} \quad \sin (\nu t + \phi_L)$$

where

$$A = \pm \left[\frac{\partial C_L}{\partial \alpha}\bigg|_o + R \frac{\partial C_L}{\partial \sigma}\bigg|_o + C_{D_o}\right] \frac{\omega \ell^{-kf}}{V}$$

$$\text{and} \quad B = \pm 2 C_{L_o} \frac{\omega \ell^{-kf}}{V} \qquad \text{(B-8)}$$

$$\text{and} \quad \phi_L = \tan^{-1} \frac{A}{B}$$

It is further assumed that any variations due to addition of a flap may be neglected provided that smooth water measurements of $\frac{\partial C_L}{\partial \alpha}\Big|_o$, $\frac{\partial C_L}{\partial \sigma}\Big|_o$, R and C_{L_o} for a foil with the requisite flap are substituted in Eqs. (B-8).

C. Theory Based on Measured Cavity Pressures

The development in Section B neglects variations in σ caused by changing velocity and submergence in waves. These are included in the following analysis.

The cavitation index σ is defined as

$$\sigma = \frac{P - P_c}{\frac{1}{2}\rho V^2} \tag{B-9}$$

Consequently, again retaining only first order terms,

$$\sigma - \sigma_o = \Delta\sigma = \left.\frac{\partial\sigma}{\partial P}\right|_o \Delta P + \left.\frac{\partial\sigma}{\partial P_c}\right|_o \Delta P_c + \left.\frac{\partial\sigma}{\partial V}\right|_o \Delta V$$

$$= \frac{2}{\rho V^2}(\Delta P - \Delta P_c) - \frac{4}{\rho V^3}(P_o - P_c)\,\Delta V$$

$$\frown\!\!\!\!\!\!\frown \frac{2g}{V^2}\left(\eta - \frac{\Delta P_c}{\gamma}\right) + 2\sigma_o\bar{u} \tag{B-10}$$

where $\Delta P_c = \Delta P_{c_m} \sin(\nu t + \phi_{p_c})$

Substituting Eq. (B-10) into Eq. (B-6)

$$C_{L_w} \frown\!\!\!\!\!\!\frown [1 - 2\bar{u} + \bar{w}\tan\alpha_g][C_{L_o} + \left.\frac{\partial C_L}{\partial\alpha}\right|_o \bar{w} + \left.\frac{\partial C_L}{\partial\sigma}\right|_o \left(\frac{2g}{V^2}\eta\right.$$

$$\left. - \frac{2g}{V^2}\frac{\Delta P_c}{\gamma} + 2\sigma_o\bar{u}\right)] \frown\!\!\!\!\!\!\frown C_{L_o} + \left.\frac{\partial C_L}{\partial\alpha}\right|_o \bar{w} + \frac{2g}{V^2}\left.\frac{\partial C_L}{\partial\sigma}\right|_o \eta$$

$$- \frac{2g}{V^2}\left.\frac{\partial C_L}{\partial\sigma}\right|_o \frac{\Delta P_c}{\gamma} + 2\sigma_o \left.\frac{\partial C_L}{\partial\sigma}\right|_o \bar{u} - 2\bar{u}\,C_{L_o} + C_{L_o}\bar{w}\tan\alpha_g$$

Hence

$$\frac{\Delta C_{L_w}}{a} = \pm\frac{\omega\ell^{-kf}}{V}\cos\nu t\left[\left.\frac{\partial C_L}{\partial\alpha}\right|_o + C_{D_o}\right]$$

$$\pm\frac{\omega\ell^{-kf}}{V}\sin\nu t\left[2C_{L_o} - 2\sigma_o\left.\frac{\partial C_L}{\partial\sigma}\right|_o\right]$$

$$+ \frac{2g}{V^2} \left.\frac{\partial C_L}{\partial \sigma}\right|_o \sin \nu t - \frac{2g}{V^2} \left.\frac{\partial C_L}{\partial \sigma}\right|_o \frac{\Delta P_{c_{m/\gamma}}}{a} \sin(\nu t + \phi_{p_c})$$

$$= \sqrt{A^2 + B^2} \quad \sin(\nu t + \phi_L)$$

where

$$A = \pm \left[\left.\frac{\partial C_L}{\partial \alpha}\right|_o + C_{D_o}\right] \frac{\omega \ell^{-kf}}{V} - \frac{2g}{V} \left.\frac{\partial C_L}{\partial \sigma}\right|_o \frac{\Delta P_{c_{m/\gamma}}}{a} \sin \phi_{p_c}$$

and

$$B = \pm \left[C_{L_o} - \sigma_o \left.\frac{\partial C_L}{\partial \sigma}\right|_o\right] \frac{\omega \ell^{-kf}}{V/2} + \frac{2g}{V^2} \left.\frac{\partial C_L}{\partial \sigma}\right|_o \left[1 - \frac{\Delta P_{c_{m/\gamma}}}{a} \cos \phi_{p_c}\right] \qquad \text{(B-11)}$$

and $\phi_L = \tan^{-1} \frac{A}{B}$

An attempt was made to predict $\Delta P_{c_m}/\lambda$ from smooth water data assuming that ϕ_{p_c} was $3\pi/2$. From smooth water curves of W (air-flow rate) against σ for varying angles of attack at fixed submergence and velocity the variation of α with σ may be crossplotted for any fixed W. From the available data only three intersections could be obtained and these with very little accuracy. This results from the very small negative slope of the W versus σ curves in the reentrant jet region and the difficulty of obtaining their precise location due to scatter of the experimental data. Computations of $\left|\frac{\Delta C_L}{a}\right|$ were unreliable and gave very poor agreement with experimental values. They are therefore not presented.

To gain some knowledge of the overall validity of the assumptions $\left|\frac{\Delta C_L}{a}\right|$ and ϕ_L were computed using experimentally obtained values of $\Delta P_{c_m}/\gamma$ and ϕ_{p_c} in waves. The results of these computations are shown in Fig. 10a, 10b, 10c, and 10d for $\delta = 0$ degrees and $\delta = 16$ degrees. It was again assumed that Eqs. (B-11) could be applied for flapped foils provided that smooth water values of $\left.\frac{\partial C_L}{\partial \alpha}\right|_o$, $\left.\frac{\partial C_L}{\partial \sigma}\right|_o$, and C_{L_o} with flaps were used.

D. Approximation for Low Cavitation Numbers

In the pulsating cavity region (low σ_o) the smooth water air-flow rate, W versus σ curves for various angles of attack and fixed submergence and velocity indicate that variations in σ with α will be small, and hence $\Delta P_{c_m}/\gamma$ will be small. If it is assumed that $\Delta P_{c_m}/a$ and $\sigma_o \frac{\partial C_L}{\partial \sigma}\Big|_o$ will be sufficiently small to be negligible at low σ_o Eqs. (B-11) may be simplified to

$$A = \pm \left[\frac{\partial C_L}{\partial \alpha}\Big|_o + C_{D_o}\right] \frac{\omega \ell^{-kf}}{V}$$

$$B = \pm 2C_{L_o} \frac{\omega \ell^{-kf}}{V} + \frac{2g}{V^2} \frac{\partial C_L}{\partial \sigma}\Big|_o$$

$$\phi_L = \tan^{-1} \frac{A}{B}$$

Bearing in mind its limitations at low angles of attack and the fact that it applies for a two-dimensional flow, the following approximation taken from Wu [12] is used for the lift coefficient when σ is small:

$$C_L \leftrightharpoons C_{L_o} (1 + \sigma) \qquad \text{(B-12)}$$

Hence
$$\left.\begin{aligned} A &= \pm \left[\frac{\partial C_L}{\partial \alpha}\Big|_o + C_{D_o}\right] \frac{\omega \ell^{-kf}}{V} \\ B &= 2C_{L_o} \left[\pm \frac{\omega \ell^{-kf}}{V} + \frac{g}{V^2}\right] \\ \phi_L &= \tan^{-1} \frac{A}{B} \end{aligned}\right\} \qquad \text{(B-13)}$$

The results of applying these approximations at $\sigma \leftrightharpoons 0$ for δ = 0 degrees and δ = 16 degrees are shown in Fig. 10a, 10b, 10c, and 10d.

However, an examination of the experimental records for σ = 0.053 when δ = 16 degrees indicates that the terms in Eqs. (B-11)

$$-0.060 < \left[1 - \frac{\Delta P_{c_{m/\gamma}}}{a} \cos \phi_{p_c}\right] < 1.000$$

for $30 > \lambda > 4$

and $$0.078 < -\frac{2g}{V^2} \left.\frac{\partial C_L}{\partial \sigma}\right|_o \frac{\Delta P_{c_{m/\gamma}}}{a} \sin \phi_{p_c} < 0.118$$

for $4 < \lambda < 10$

and $$0.057 < -\frac{2g}{V^2} \left.\frac{\partial C_L}{\partial \sigma}\right|_o \frac{\Delta P_{c_{m/\gamma}}}{a} \sin \phi_{p_c} < 0.118$$

for $30 > \lambda > 10$

Thus, regardless of the fact that they give reasonable agreement with experimental values, the assumptions of this section cannot be justified in light of the cavity pressure variation amplitude and phase measurements.

E. Variation of $\Delta\sigma$ with $\Delta\alpha$ in Waves

From Eq. (B-10)

$$\Delta\sigma = \left\{ \frac{2g}{V^2} a - \frac{2g}{V^2} \frac{\Delta P_{c_m}}{\gamma} \cos \phi_{p_c} \mp \frac{2\sigma_o a}{V} \omega\ell^{-kf} \right\} \sin \nu t$$

$$+ \left\{ \frac{-2g}{V^2} \frac{\Delta P_{c_m}}{\gamma} \sin \phi_{p_c} \right\} \cos \nu t$$

$$= \left|\Delta\sigma\right| \sin (\nu t + \phi_\sigma)$$

where $\left|\Delta\sigma\right| = \sqrt{A^2 + B^2}$

and
$$\left.\begin{aligned} A &= \frac{-2g}{V^2} \frac{\Delta P_{c_m}}{\gamma} \sin \phi_{p_c} \\ B &= \frac{2g}{V^2} a - \frac{2g}{V^2} \frac{\Delta P_{c_m}}{\gamma} \cos \phi_{p_c} \mp \frac{2\sigma_o a}{V} \omega\ell^{-kf} \end{aligned}\right\} \quad \text{(B-14)}$$

and $\phi_\sigma = \tan^{-1} \frac{A}{B}$

Also $\Delta\alpha \leftrightarrow \bar{w} = \frac{a\omega\ell^{-kf}}{V} \sin(\nu t + \frac{\pi}{2}) = \left|\Delta\alpha\right| \sin(\nu t + \frac{\pi}{2})$

Hence $\Delta\sigma$ leads $\Delta\alpha$ by $(\phi_\sigma - \frac{\pi}{2})$ (B-15)

Hence $\cos \nu t = \frac{\Delta\alpha}{\left|\Delta\alpha\right|}$

$$\Delta\sigma = \left|\Delta\sigma\right| \left\{\sin \nu t \cos \phi_\sigma + \cos \nu t \sin \phi_\sigma\right\}$$

$$= \left|\Delta\sigma\right| \left\{\left[1 - \left(\frac{\Delta\alpha}{\left|\Delta\alpha\right|}\right)^2\right]^{1/2} \cos \phi_\sigma + \frac{\Delta\alpha}{\left|\Delta\alpha\right|} \sin \phi_\sigma\right\} \quad \text{(B-16)}$$

Now, for a given λ and a, knowing the experimental values of V, $\frac{\Delta P_{c_m}}{\gamma}$, ϕ_{p_c}, and σ_o it is noted that $\left|\Delta\sigma\right|$, ϕ_σ, and $\left|\Delta\alpha\right|$ can be computed using Eqs. (B-14) and (B-15). Equation (B-16) then indicates that a separate relationship between $\Delta\alpha$ and $\Delta\sigma$ exists for each value of λ and a.

This, then, gives some indication of the limitations of the assumption in Eq. (B-7).

F. Drag in Waves

Under the same assumptions applied to obtain $\frac{\Delta C_{L_w}}{a}$ it can readily be shown that

$$\left|\frac{\Delta C_{D_w}}{a}\right| = \left|\frac{\Delta C_L}{a}\right| \tan \alpha_g$$

and $\phi_D = \phi_L$

A P P E N D I X C

Tabular Summary of Experimental Data

WEDGE FLAT PLATE--RECTANGULAR PLANFORM

3 in. chord; 12 in. span

V fps	f in.	c_f/c	α deg.	δ deg.	W x 10^3 lbs/sec/in^2	c_a	C_L	C_D	σ
12	3	0.25	10	8	.113	--	.341	.067	.064
					.154	--	.341	.067	.067
					.194	--	.373	.067	.067
					.229	--	.354	.067	.067
					.309	--	.373	.069	.070
					.270	--	.373	.069	.073
					.091	--	.361	.069	.095
					.105	.397	.361	.067	.100
					.074	.388	.405	.077	.145
					.070	.350	.448	.086	.198
					.059	.321	.490	.094	.255
					.052	.260	.532	.100	.280
					.043	.217	.557	.106	.331
16	1.5	0.25	7	16	.313	--	.403	.072	.037
					.272	--	.407	.072	.039
					.233	--	.407	.072	.043
					.194	--	.419	.073	.051
					.176	--	.407	.074	.065
					.158	--	.425	.077	.079
					.137	--	.419	.077	.086
					.118	.406	.480	.084	.139
					.098	.353	.502	.089	.213
					.088	.300	.550	.103	.305
16	3	0.25	7	16	.315	--	.381	.075	.046
					.283	--	.381	.073	.046
					.250	--	.381	.075	.046
					.210	--	.381	.075	.051
					.188	--	.408	.073	.052
					.168	--	.420	.076	.057
					.150	--	.408	.079	.093
					.126	.421	.445	.084	.132
					.113	.397	.455	.085	.205
					.101	.359	.504	.091	.267
16	6	0.25	7	16	.313	--	.381	.076	.049
					.272	--	.381	.076	.051
					.233	--	.396	.076	.056
					.195	--	.396	.076	.060
					.168	--	.408	.080	.086
					.158	.486	.420	.081	.102
					.138	.440	.453	.086	.139
					.121	.389	.504	.095	.226
					.099	.315	.577	.110	.323

WEDGE FLAT PLATE--RECTANGULAR PLANFORM

3 in. chord; 12 in. span

V fps	f in.	c_f/c	α deg.	δ deg.	W x 10^3 lbs/sec/in^2	c_a	C_L	C_D	σ
16	3	--	8	0	.289	--	.168	.030	.046
					.201	--	.168	.028	.047
					.138	--	.168	.026	.047
					.100	--	.168	.026	.051
					.065	--	.174	.030	.060
					.056	--	.180	.028	.074
					.048	.427	.185	.031	.079
					.051	.441	.185	.031	.083
					.038	.360	.203	.033	.111
					.042	.369	.210	.033	.125
					.043	.307	.321	.048	.196
					.047	.311	.330	.052	.201
					.047	.311	.336	.051	.201
					.039	.251	.324	.059	.214
16	3	0.25	8	4	.319	--	.240	.037	.039
					.272	--	.240	.037	.039
					.233	--	.240	.037	.039
					.195	--	.240	.037	.039
					.158	--	.240	.037	.039
					.139	--	.240	.039	.039
					.117	--	.240	.042	.040
					.108	--	.240	.041	.042
					.098	--	.245	.041	.044
					.087	.500	.245	.042	.052
					.076	.468	.264	.042	.088
					.069	.429	.263	.045	.115
					.066	.400	.286	.048	.141
					.063	.404	.281	.046	.153
					.062	.365	.324	.053	.189
					.056	.298	.396	.067	.278
					.049	.270	.396	.067	.297
16	3	0.25	8	8	.320	--	.299	.050	.042
					.268	--	.299	.050	.042
					.230	--	.299	.050	.042
					.180	--	.299	.050	.042
					.120	--	.299	.050	.051
					.107	--	.314	.053	.070
					.097	.458	.317	.055	.093
					.099	.465	.317	.055	.097
					.084	.403	.341	.060	.120
					.072	.360	.358	.063	.157
					.080	.339	.437	.079	.269
					.069	.299	.450	.082	.287

WEDGE FLAT PLATE--RECTANGULAR PLANFORM

3 in. chord; 12 in. span

V fps	f in.	c_f/c	α deg.	δ deg.	W x 10^3 lbs/sec/in^2	c_a	C_L	C_D	σ
16	3	0.25	8	12	.179	--	.372	.065	.069
					.146	--	.359	.068	.078
					.126	--	.372	.065	.088
					.129	--	.383	.065	.098
					.107	.413	.420	.075	.161
					.102	.393	.420	.078	.166
					.089	.360	.444	.078	.210
					.070	.268	.564	.098	.322
16	3	0.25	8	16	.315	--	.406	.086	.056
					.290	--	.406	.086	.056
					.240	--	.406	.086	.063
					.200	--	.418	.088	.072
					.181	--	.430	.088	.084
					.160	.455	.442	.092	.106
					.146	.430	.454	.095	.153
					.123	.371	.501	.103	.213
					.100	.290	.597	.123	.331
16	3	0.25	8	20	.268	--	.504	.100	.061
					.244	--	.504	.100	.078
					.225	--	.504	.105	.078
					.202	.480	.524	.106	.098
					.190	.469	.528	.105	.109
					.185	.450	.551	.110	.141
					.162	.420	.570	.111	.184
					.148	.381	.600	.119	.204
					.137	.345	.648	.132	.282
16	3	0.50	8	8	.250	--	.359	.068	.059
					.207	--	.359	.066	.059
					.190	--	.372	.071	.068
					.155	--	.372	.064	.088
					.130	.470	.396	.073	.103
					.117	.423	.419	.079	.132
					.100	.370	.456	.085	.195
					.086	.296	.564	.105	.316
16	3	0.50	8	16	.302	--	.480	.117	.078
					.279	--	.480	.117	.088
					.247	.502	.492	.121	.108
					.227	.470	.516	.124	.127
					.214	.450	.528	.131	.157
					.202	.447	.552	.131	.177
					.198	.413	.565	.141	.196
					.169	.364	.625	.151	.275
					.160	.348	.636	.154	.304

WEDGE FLAT PLATE--RECTANGULAR PLANFORM

3 in. chord; 12 in. span

V fps	f in.	c_f/c	α deg.	δ deg.	W x 10^3 lbs/sec/in^2	c_a	C_L	C_D	σ
16	3	--	10	12	3.51	--	.209	.050	.058
					3.33	--	.214	.047	.067
					3.06	--	.224	.053	.095
					2.84	--	.229	.055	.111
					2.87	.398	.260	.060	.139
					2.93	.415	.245	.057	.148
					2.86	.406	.250	.058	.155
					2.80	.393	.255	.060	.176
					2.82	.376	.296	.066	.220
					2.75	.359	.306	.069	.233
					2.74	.346	.326	.073	.258
					2.53	.327	.331	.074	.265
					2.67	.342	.337	.073	.272
					2.28	.282	.359	.083	.301
					2.34	.295	.342	.080	.304
					2.60	.303	.393	.086	.346
16	3	0.25	10	4	10.5	--	.240	.052	.046
					10.9	--	.250	.060	.049
					3.54	--	.245	.051	.079
					3.80	--	.280	.068	.112
					3.10	.416	.286	.060	.152
					3.34	.389	.306	.073	.175
					3.21	.378	.326	.074	.203
					2.84	.367	.336	.069	.227
					2.79	.354	.352	.072	.252
					2.53	.316	.387	.078	.288
					2.86	.318	.408	.088	.312
					1.65	.214	.460	.087	.341
					2.47	.277	.438	.093	.345
16	3	0.25	10	8	.307	--	.330	.066	.046
					.226	--	.330	.066	.046
					.290	--	.323	.066	.047
					.255	--	.330	.066	.047
					.226	--	.323	.066	.049
					.205	--	.330	.066	.051
					.192	--	.335	.066	.051
					.196	--	.323	.066	.054
					.176	--	.330	.066	.058
					.150	.510	.344	.070	.081
					.144	.500	.349	.069	.086
					.146	.506	.344	.069	.088
					.134	.468	.371	.074	.139
					.120	.441	.382	.074	.143
					.101	.374	.431	.085	.221
					.091	.330	.515	.094	.314

WEDGE FLAT PLATE--RECTANGULAR PLANFORM

3 in. chord; 12 in. span

V fps	f in.	c_f/c	α deg.	δ deg.	W x 10^3 lbs/sec/in^2	c_a	C_L	C_D	σ
16	3	0.25	10	12	.203	--	.407	.085	.073
					.207	--	.420	.085	.083
					.176	.485	.432	.091	.109
					.153	.436	.456	.098	.146
					.140	.403	.491	.105	.195
					.125	.363	.528	.111	.235
					.112	.316	.588	.125	.312
16	3	0.25	10	16	.318	--	.430	.102	.058
					.295	--	.441	.102	.060
					.274	--	.441	.106	.067
					.256	--	.441	.106	.072
					.238	--	.455	.108	.074
					.198	.459	.479	.115	.115
					.177	.428	.503	.118	.169
					.167	.396	.539	.128	.207
					.145	.365	.540	.128	.223
					.129	.318	.614	.142	.295
					.120	.293	.647	.150	.331
16	3	0.25	10	20	.300	--	.528	.119	.078
					.281	--	.540	.121	.088
					.253	--	.540	.126	.098
					.235	.468	.540	.132	.119
					.220	.453	.551	.132	.136
					.202	.414	.588	.145	.180
					.188	.396	.600	.145	.200
					.165	.359	.624	.150	.241
					.129	.278	.744	.174	.356
16	3	0.50	10	8	.289	--	.396	.085	.059
					.254	--	.408	.090	.059
					.221	--	.408	.085	.078
					.185	.499	.419	.092	.107
					.173	.465	.432	.098	.115
					.156	.426	.466	.105	.184
					.142	.381	.515	.116	.200
					.132	.376	.515	.111	.210
16	3	0.50	10	16	.300	.507	.517	.144	.108
					.275	.480	.528	.148	.132
					.265	.465	.528	.151	.137
					.247	.450	.541	.151	.162
					.228	.411	.565	.164	.201
					.220	.403	.576	.164	.216
					.205	.380	.625	.171	.254
					.192	.353	.660	.181	.313

WEDGE FLAT PLATE--RECTANGULAR PLANFORM

3 in. chord; 12 in. span

V fps	f in.	c_f/c	α deg.	δ deg.	W x 10^3 lbs/sec/in^2	c_a	C_L	C_D	σ
16	1.5	0.25	14	16	.313	--	.521	.150	.107
					.295	--	.521	.150	.111
					.278	.468	.529	.156	.136
					.255	.443	.539	.161	.157
					.235	.422	.550	.161	.166
					.220	.398	.574	.166	.185
					.210	.377	.599	.175	.208
					.197	.355	.623	.182	.240
					.191	.340	.649	.188	.286
					.177	.310	.682	.204	.315
16	3	--	14	0	7.63	--	.270	.077	.049
					6.39	--	.286	.080	.059
					6.10	--	.288	.083	.082
					5.71	.487	.332	.083	.152
					5.14	.445	.346	.089	.178
					4.86	.413	.306	.096	.178
					5.15	.425	.337	.097	.182
					4.81	.407	.336	.098	.215
					4.50	.371	.377	.107	.219
					4.81	.381	.383	.110	.230
					4.58	.363	.408	.114	.278
					3.88	.300	.470	.130	.337
					3.85	.293	.469	.134	.345
16	3	0.25	14	4	12.20	--	.306	.092	.055
					10.90	--	.311	.095	.067
					8.90	--	.316	.096	.071
					7.25	--	.336	.096	.108
					6.95	.494	.326	.098	.122
					6.59	.469	.378	.104	.186
					5.60	.389	.419	.123	.209
					5.40	.378	.408	.125	.238
					5.40	.372	.428	.129	.252
					5.26	.346	.489	.142	.294
					5.07	.342	.485	.139	.294
					4.87	.323	.500	.146	.307
					5.12	.342	.480	.141	.314
					5.05	.333	.490	.145	.330
					4.66	.308	.490	.151	.350
					4.58	.304	.520	.151	.351
					3.90	.253	.575	.166	.356

WEDGE FLAT PLATE--RECTANGULAR PLANFORM

3 in. chord; 12 in. span

V fps	f in.	c_f/c	α deg.	δ deg.	W x 10^3 lbs/sec/in^2	c_a	C_L	C_D	σ
16	3	0.25	14	8	.320	--	.383	.100	.063
					.270	--	.389	.100	.072
					.230	--	.400	.103	.086
					.220	.471	.460	.122	.148
					.201	.456	.479	.119	.157
					.202	.460	.480	.119	.175
					.183	.424	.501	.126	.203
					.177	.413	.490	.126	.208
					.135	.315	.599	.151	.310
16	3	0.25	14	12	.315	--	.480	.132	.084
					.295	--	.480	.132	.096
					.306	--	.456	.125	.098
					.272	--	.490	.138	.110
					.278	--	.469	.128	.112
					.252	.475	.490	.138	.130
					.249	.517	.491	.131	.137
					.235	.448	.529	.145	.156
					.224	.450	.504	.138	.176
					.215	.424	.551	.148	.187
					.198	.389	.561	.157	.209
					.202	.410	.553	.148	.216
					.187	.366	.599	.164	.256
					.179	.366	.588	.158	.264
					.175	.332	.620	.172	.281
					.170	.337	.640	.172	.325
					.159	.310	.659	.184	.345
					.151	.305	.660	.178	.352
16	3	0.25	14	16	.314	.490	.529	.161	.118
					.293	.471	.529	.164	.127
					.295	.467	.551	.166	.130
					.272	.447	.532	.167	.147
					.275	.440	.551	.173	.155
					.252	.420	.551	.174	.167
					.255	.420	.578	.176	.176
					.232	.402	.575	.174	.191
					.239	.410	.578	.173	.195
					.225	.393	.588	.176	.213
					.214	.365	.599	.188	.235
					.210	.362	.634	.188	.280
					.205	.327	.651	.218	.320
16	3	0.25	14	20	.301	.445	.612	.185	.148
					.283	.430	.623	.185	.165
					.250	.383	.668	.200	.206
					.219	.349	.684	.205	.224
					.195	.303	.780	.230	.342

WEDGE FLAT PLATE--RECTANGULAR PLANFORM

3 in. chord; 12 in. span

(continued)

V fps	f in.	c_f/c	α deg.	δ deg.	W x 10^3 lbs/sec/in^2	c_a	C_L	C_D	σ
16	3	0.25	14	6	.293	---	.382	.106	.069
					.253	---	.383	.106	.081
					.230	.505	.402	.110	.110
					.205	.472	.418	.114	.132
					.194	.452	.430	.117	.145
					.185	.435	.442	.122	.167
					.175	.410	.479	.126	.196
					.165	.391	.479	.130	.205
					.155	.368	.485	.134	.215
					.146	.346	.515	.140	.255
					.137	.311	.573	.157	.331

WEDGE FLAT PLATE--RECTANGULAR PLANFORM

3 in. chord; 12 in. span

V fps	f in.	c_f/c	α deg.	δ deg.	W x 10^3 lbs/sec/in^2	c_a	C_L	C_D	σ
16	3	0.50	14	8	.300	--	.467	.135	.103
					.277	.497	.480	.138	.119
					.245	.458	.504	.145	.165
					.218	.421	.529	.151	.195
					.209	.397	.553	.160	.224
					.197	.391	.529	.156	.228
					.161	.306	.648	.190	.352
16	3	0.50	14	16	.305	.425	.600	.204	.196
					.288	.399	.624	.217	.216
					.273	.380	.649	.221	.240
					.261	.360	.685	.231	.294
					.250	.359	.696	.231	.345
16	1.5	0.25	18	16	.310	.405	.611	.227	.194
					.293	.387	.622	.233	.216
					.271	.370	.636	.233	.240
					.241	.320	.742	.250	.260
16	3	--	18	0	.315	--	.359	.113	.086
					.309	--	.359	.113	.086
					.301	--	.370	.114	.088
					.271	--	.384	.114	.104
					.259	.525	.384	.116	.116
					.235	.473	.396	.130	.139
					.221	.470	.413	.126	.176
					.189	.409	.456	.138	.232
					.167	.325	.575	.179	.346
16	3	0.25	18	4	.307	--	.431	.158	.092
					.270	.470	.456	.150	.113
					.253	.423	.466	.172	.158
					.232	.420	.490	.161	.186
					.213	.381	.539	.175	.224
					.205	.382	.535	.169	.246
					.193	.359	.562	.177	.295
					.185	.344	.588	.182	.318
16	3	0.25	18	6	.293	.466	.480	.168	.140
					.258	.430	.514	.171	.176
					.252	.425	.514	.171	.186
					.232	.381	.539	.178	.206
					.224	.374	.551	.191	.236
					.215	.362	.575	.191	.250
					.194	.309	.637	.225	.345

WEDGE FLAT PLATE--RECTANGULAR PLANFORM

3 in. chord; 12 in. span

V fps	f in.	c_f/c	α deg.	δ deg.	W x 10^3 lbs/sec/in^2	c_a	C_L	C_D	σ
16	3	0.25	18	8	.315	.485	.479	.165	.124
					.272	.444	.528	.170	.161
					.300	.469	.528	.170	.171
					.259	.416	.550	.182	.203
					.221	.384	.562	.181	.221
					.220	.355	.631	.205	.296
16	3	0.25	18	12	.330	.447	.576	.203	.151
					.295	.408	.612	.214	.201
					.273	.385	.627	.218	.215
					.254	.364	.649	.226	.254
					.234	.328	.695	.246	.319
					.215	.294	.734	.267	.356
16	3	0.25	18	16	.300	.367	.671	.264	.278
18	3	0.25	10	8	.309	--	.319	.065	.041
					.196	.550	.341	.069	.103

WEDGE FLAT PLATE--RECTANGULAR PLANFORM

3 in. chord; 18 in. span

V fps	f in.	c_f/c	α deg.	δ deg.	W x 10^3 lbs/sec/in^2	c_a	C_L	C_D	σ
16	3	--	8	0	.144	--	.184	.028	.108
					.125	--	.184	.028	.108
					.092	--	.193	.030	.121
					.108	--	.192	.032	.138
					.083	.560	.200	.032	.156
					.075	.518	.208	.034	.161
					.066	.490	.225	.034	.208
					.057	.424	.281	.039	.281
16	3	0.25	8	8	.176	--	.320	.052	.065
					.167	--	.320	.052	.069
					.147	--	.320	.052	.069
					.140	--	.328	.054	.087
					.128	.527	.336	.056	.091
					.119	.510	.344	.056	.108
					.110	.464	.368	.063	.130
					.102	.438	.401	.065	.164
					.095	.400	.425	.070	.200
					.084	.345	.481	.081	.252
16	3	0.25	8	16	.201	--	.481	.092	.094
					.182	.494	.490	.092	.108
					.174	.477	.501	.094	.112
					.164	.464	.501	.094	.126
					.154	.432	.541	.101	.162
					.145	.413	.541	.103	.180
					.136	.384	.599	.110	.224
					.127	.362	.622	.114	.251
					.119	.339	.641	.119	.278
					.101	.289	.682	.128	.306
					.092	.272	.624	.130	.322
16	3	--	10	0	.183	--	.224	.044	.027
					.248	--	.234	.044	.035
					.152	--	.240	.044	.041
					.344	--	.234	.044	.046
					.131	--	.240	.044	.050
					.113	--	.248	.046	.050
					.146	--	.248	.045	.067
					.134	--	.248	.045	.069
					.126	--	.256	.043	.074
					.117	--	.248	.045	.082
					.108	--	.256	.043	.087
					.104	.510	.258	.049	.100
					.098	.477	.281	.053	.101
					.100	.509	.264	.048	.104
					.098	.462	.305	.057	.164

WEDGE FLAT PLATE--RECTANGULAR PLANFORM

3 in. chord; 18 in. span

V fps	f in.	c_f/c	α deg.	δ deg.	W x 10^3 lbs/sec/in^2	c_a	C_L	C_D	σ
16	3	--	10	0	.092	.458	.337	.057	.164
					.093	.429	.336	.063	.197
					.085	.392	.370	.067	.219
					.077	.387	.416	.061	.225
					.068	.315	.432	.074	.248
					.081	.371	.394	.071	.252
					.074	.341	.410	.073	.264
					.069	.311	.425	.078	.286
16	3	0.25	10	8	.203	--	.369	.077	.082
					.184	--	.369	.073	.082
					.166	.524	.385	.074	.099
					.155	.508	.385	.074	.108
					.146	.486	.401	.077	.126
					.137	.450	.401	.083	.148
					.129	.427	.434	.088	.179
					.110	.357	.511	.101	.252
					.104	.333	.511	.106	.259
					.094	.303	.529	.110	.287
16	3	0.25	10	16	.239	.516	.501	.110	.103
					.221	.495	.520	.112	.126
					.201	.466	.541	.114	.148
					.182	.425	.581	.123	.197
					.165	.389	.641	.132	.251
					.147	.345	.682	.143	.291
					.128	.309	.624	.148	.314
16	6	--	10	0	.342	--	.236	.045	.062
					.295	--	.232	.045	.062
					.249	--	.232	.045	.062
					.200	--	.232	.045	.062
					.151	--	.240	.045	.074
					.139	--	.249	.047	.083
					.126	--	.249	.045	.083
					.112	--	.249	.047	.088
					.103	.498	.264	.052	.097
					.099	.475	.288	.054	.134
					.088	.389	.401	.073	.229
					.094	.430	.375	.073	.240
					.091	.393	.385	.071	.240
					.086	.365	.415	.076	.240
					.085	.362	.408	.076	.240
					.081	.343	.408	.081	.275
					.080	.347	.433	.078	.297
					.074	.318	.440	.082	.309
					.075	.308	.440	.087	.321

WEDGE FLAT PLATE--RECTANGULAR PLANFORM

3 in. chord; 18 in. span

V fps	f in.	c_f/c	α deg.	δ deg.	W x 10^3 lbs/sec/in^2	c_a	C_L	C_D	σ
16	3	--	14	0	.343	--	.315	.078	.055
					.295	--	.315	.078	.062
					.251	--	.318	.078	.069
					.200	--	.320	.081	.088
					.192	--	.344	.083	.095
					.182	--	.344	.083	.095
					.172	--	.352	.083	.100
					.176	--	.337	.085	.102
					.173	--	.337	.085	.109
					.165	--	.360	.086	.113
					.166	--	.345	.085	.115
					.146	.436	.385	.092	.123
					.154	.465	.369	.088	.125
					.161	.476	.352	.088	.128
					.157	.468	.345	.088	.133
					.151	.440	.385	.096	.165
					.146	.432	.385	.096	.174
					.136	.407	.416	.099	.190
					.127	.369	.464	.110	.252
					.131	.367	.465	.116	.275
					.125	.344	.498	.123	.308
					.120	.331	.507	.125	.322
					.114	.305	.530	.134	.345
16	3	0.25	14	8	.221	.474	.465	.123	.156
					.211	.454	.481	.127	.174
					.201	.442	.489	.127	.174
					.192	.423	.504	.132	.199
					.184	.397	.559	.141	.217
					.174	.358	.602	.159	.257
					.165	.347	.640	.159	.281
					.157	.312	.640	.168	.305
					.146	.282	.672	.190	.326
16	3	0.25	14	16	.275	.445	.599	.169	.172
					.259	.426	.599	.176	.188
					.240	.394	.641	.185	.224
					.220	.368	.682	.194	.270
					.201	.330	.762	.207	.306

WEDGE FLAT PLATE--RECTANGULAR PLANFORM

3 in. chord; 18 in. span

V fps	f in.	c_f/c	α deg.	δ deg.	W x 10^3 lbs/sec/in^2	c_a	C_L	C_D	σ
16	6	--	14	0	.341	--	.305	.076	.073
					.295	--	.295	.073	.073
					.247	--	.305	.076	.073
					.200	--	.320	.081	.092
					.177	.509	.334	.084	.118
					.160	.472	.355	.089	.146
					.162	.476	.355	.089	.170
					.156	.458	.368	.093	.183
					.128	.342	.465	.128	.344
					.123	.324	.497	.134	.355
					.119	.324	.490	.130	.355
16	3	--	18	0	.342	--	.369	.128	.091
					.317	--	.380	.132	.100
					.283	.512	.381	.133	.108
					.277	.497	.398	.139	.126
					.260	.486	.425	.136	.146
					.250	.444	.447	.157	.174
					.236	.449	.450	.146	.183
					.223	.413	.450	.160	.200
					.212	.401	.496	.160	.239
					.185	.312	.601	.187	.328
16	6	--	18	0	.342	.560	.393	.133	.110
					.294	.515	.410	.137	.132
					.248	.452	.445	.151	.195
					.223	.413	.480	.160	.220
					.198	.362	.530	.183	.297

SPONSOR'S DISTRIBUTION LIST FOR PROJECT REPORT NO. 66

of the St. Anthony Falls Hydraulic Laboratory

Copies	Organization
6	Chief of Naval Research, Department of the Navy, Washington 25, D. C. Attn: 3 - Code 438 1 - Code 461 1 - Code 463 1 - Code 466
1	Commanding Officer, Office of Naval Research, Branch Office, 495 Summer Street, Boston 10, Massachusetts.
1	Commanding Officer, Office of Naval Research, Branch Office, 207 West 24th Street, New York 11, New York.
1	Commanding Officer, Office of Naval Research, Branch Office, 1030 East Green Street, Pasadena, California.
1	Commanding Officer, Office of Naval Research, Branch Office, 1000 Geary Street, San Francisco 9, California.
25	Commanding Officer, Office of Naval Research, Branch Office, Box 39, Navy 100, Fleet Post Office, New York, New York.
6	Director, Naval Research Laboratory, Washington 25, D. C. Attn: Code 2027.
5	Chief, Bureau of Naval Weapons, Department of the Navy, Washington 25, D. C. Attn: 1 - Code RUAW-4 1 - Code RRRE 1 - Code RAAD 1 - Code RAAD-222 1 - Code DIS-42
8	Chief, Bureau of Ships, Department of the Navy, Washington 25, D. C. Attn: 1 - Code 310 1 - Code 312 1 - Code 335 1 - Code 420 1 - Code 421 1 - Code 440 1 - Code 442 1 - Code 449
1	Chief, Bureau of Yards and Docks, Department of the Navy, Washington 25, D. C. Attn: Code D-400.

Copies	Organization
16	Commanding Officer and Director, David Taylor Model Basin, Washington 7, D. C. Attn: 1 - Code 108 1 - Code 142 1 - Code 500 1 - Code 513 1 - Code 520 1 - Code 525 1 - Code 526 1 - Code 526A 1 - Code 530 1 - Code 533 1 - Code 580 1 - Code 585 1 - Code 589 1 - Code 591 1 - Code 591A 1 - Code 700
1	Commander, U.S. Naval Ordnance Test Station, China Lake, California. Attn: Code 753.
2	Commander, U. S. Naval Ordnance Test Station, Pasadena Annex, 3202 E. Foothill Blvd., Pasadena 8, California. Attn: 1 - Code P-508.
1	Commander, Planning Department, Portsmouth Naval Shipyard, Portsmouth, New Hampshire.
1	Commander, Planning Department, Boston Naval Shipyard, Boston 29, Massachusetts.
1	Commander, Planning Department, Pearl Harbor Naval Shipyard, Navy 128, Fleet Post Office, San Francisco, California.
1	Commander, Planning Department, San Francisco Naval Shipyard, San Francisco 24, California.
1	Commander, Planning Department, Mare Island Naval Shipyard, Vallejo, California.
1	Commander, Planning Department, New York Naval Shipyard, Brooklyn 1, New York.
1	Commander, Planning Department, Puget Sound Naval Shipyard, Bremerton, Washington.
1	Commander, Planning Department, Philadelphia Naval Shipyard, U. S. Naval Base, Philadelphia 12, Pennsylvania.
1	Commander, Planning Department, Norfolk Naval Shipyard, Portsmouth, Virginia.

Copies	Organization
1	Commander, Planning Department, Charleston Naval Shipyard, U. S. Naval Base, Charleston, South Carolina.
1	Commander, Planning Department, Long Beach Naval Shipyard, Long Beach 2, California.
1	Commander, Planning Department, U. S. Naval Weapons Laboratory, Dahlgren, Virginia.
1	Commander, U. S. Naval Ordnance Laboratory, White Oak, Maryland.
1	Dr. A. V. Hershey, Computation and Exterior Ballistics Laboratory, U. S. Naval Weapons Laboratory, Dahlgren, Virginia.
1	Superintendent, U. S. Naval Academy, Annapolis, Maryland, Attn: Library.
1	Superintendent, U.S. Naval Postgraduate School, Monterey, California.
1	Commandant, U. S. Coast Guard, 1300 E. Street, N. W., Washington, D. C.
1	Secretary Ship Structure Committee, U. S. Coast Guard Headquarters, 1300 E Street, N. W., Washington, D. C.
1	Commander, Military Sea Transportation Service, Department of the Navy, Washington 25, D. C.
2	U. S. Maritime Administration, GAO Building, 441 G Street, N. W., Washington, D. C. Attn: 1 - Division of Ship Design 1 - Division of Research
1	Superintendent, U. S. Merchant Marine Academy, Kings Point, Long Island, New York. Attn: 1 - Capt. L. S. McCready (Dept. of Engineering)
1	Commanding Officer and Director, U. S. Navy Mine Defense Laboratory, Panama City, Florida.
1	Commanding Officer, NROTC and Naval Administrative Unit, Massachusetts Institute of Technology, Cambridge 39, Massachusetts.
1	U. S. Army Transportation Research and Development Command, Fort Eustis, Virginia. Attn: Marine Transport Division.
1	Mr. J. B. Parkinson, National Aeronautics and Space Administration, 1512 H Street, N. W., Washington 25, D. C.
2	Director, Langley Research Center, Langley Station, Hampton, Virginia. Attn: 1 - Mr. I. E. Garrick 1 - Mr. D. J. Marten

Copies	Organization
1	Director Engineering Sciences Division, National Science Foundation, 1951 Constitution Avenue, N. W., Washington 25, D. C.
3	Director, National Bureau of Standards, Washington 25, D. C. Attn: 1 - Fluid Mechanics Division (Dr. G. B. Schubauer) 1 - Dr. G. H. Keulegan 1 - Dr. J. M. Franklin
10	Defense Documentation Center, Arlington Hall Station, Arlington 12, Virginia.
1	Office of Technical Services, Department of Commerce, Washington 25, D. C.
3	California Institute of Technology, Pasadena 4, California. Attn: 1 - Professor M. S. Plesset 1 - Professor T. Y. Wu 1 - Professor A. J. Acosta
1	University of California, Department of Engineering, Los Angeles 24, California, Attn: 1 - Dr. A. Powell
1	Director, Scripps Institute of Oceanography, University of California, La Jolla, California.
1	Professor M. L. Albertson, Department of Civil Engineering, Colorado A and M College, Fort Collins, Colorado.
1	Professor J. E. Cermak, Department of Civil Engineering, Colorado State University, Fort Collins, Colorado.
1	Professor W. R. Sears, Graduate School or Aeronautical Engineering, Cornell University, Ithaca, New York.
2	State University of Iowa, Iowa Institute of Hydraulic Research, Iowa City, Iowa. Attn: 1 - Dr. H. Rouse 1 - Dr. L. Landweber
2	Harvard University, Cambridge 38, Massachusetts. Attn: 1 - Professor G. Birkhoff (Dept. of Mathematics) 1 - Professor G. F. Carrier (Dept. of Mathematics)
2	Massachusetts Institute of Technology, Cambridge 39, Massachusetts. Attn: 1 - Department of Naval Architecture and Marine Engineering 1 - Professor A. T. Ippen
3	University of Michigan, Ann Arbor, Michigan. Attn: 1 - Professor R. B. Couch (Dept. of Naval Architecture) 1 - Professor W. W. Willmarth (Aero. Engrg. Department) 1 - Professor M. S. Uberoi (Aero. Engrg. Department)

Copies	Organization
3	Dr. L. G. Straub, Director, St. Anthony Falls Hydraulic Laboratory, University of Minnesota, Minneapolis 14, Minnesota. Attn: 1 - Mr. J. M. Wetzel 1 - Professor E. Silberman
1	Professor J. J. Foody, Engineering Department, New York State University Maritime College, Fort Schulyer, New York.
2	New York University, Institute of Mathematical Sciences, 25 Waverly Place, New York 3, New York. Attn: 1 - Professor J. Keller 1 - Professor J. J. Stoker
3	The Johns Hopkins University, Department of Mechanical Engineering, Baltimore 18, Maryland. Attn: 1 - Professor S. Corrsin 2 - Professor O. M. Phillips
1	Massachusetts Institute of Technology, Department of Naval Architecture and Marine Engineering, Cambridge 39, Massachusetts. Attn: Professor M. A. Abkowitz, Head.
2	Dr. G. F. Wislicenus, Ordnance Research Laboratory, Pennsylvania State University, University Park, Pennsylvania. Attn: Dr. M. Sevik.
1	Professor R.C. DiPrima, Department of Mathematics, Rensselaer Polytechnic Institute, Troy, New York.
4	Stevens Institute of Technology, Davidson Laboratory, Castle Point Station, Hoboken, New Jersey. Attn: 1 - Mr. D. Savitsky 1 - Mr. J. P. Breslin 1 - Mr. C. J. Henry 1 - Mr. S. Tsakonas
2	Webb Institute of Naval Architecture, Crescent Beach Road, Glen Cove, New York. Attn: 1 - Professor E. V. Lewis 1 - Technical Library
1	Director, Woods Hole Oceanographic Institute, Woods Hole, Massachusetts.
1	Executive Director, Air Force Office of Scientific Research, Washington 25, D. C. Attn: Mechanics Branch.
1	Commander, Wright Air Development Division, Aircraft Laboratory, Wright-Patterson Air Force Base, Ohio. Attn: Mr. W. Mykytow, Dynamics Branch.
2	Cornell Aeronautical Laboratory, 4455 Genesee Street, Buffalo, New York. Attn: 1 - Mr. W. Targoff 1 - Mr. R. White

Copies	Organization
3	Massachusetts Institute of Technology, Fluid Dynamics Research Laboratory, Cambridge 39, Massachusetts. Attn: 1 - Professor H. Ashley 1 - Professor M. Landahl 1 - Professor J. Dugundji
2	Hamburgische Schiffbau - Versuchsanstalt, Bramfelder Strasse 164, Hamburg 33, Germany. Attn; 1 - Dr. O. Grim 1 - Dr. H. W. Lerbs
1	Institut für Schiffbau der Universitat Hamburg, Berliner Tor 21, Hamburg 1, Germany. Attn; Prof. G. P. Weinblum, Director.
1	Transportation Technical Research Institute, 1-1057, Mejiro-Cho, Toshima-Ku, Tokyo, Japan.
1	Max-Planck Institut für Strömungsforschung, Bottingerstrasse 6/8, Gottingen, Germany. Attn: Dr. H. Reichardt.
1	Hydro-og Aerodynamisk Laboratorium, Lyngby, Denmark. Attn: Professor Carl Prohaska.
1	Skipsmodelltanken, Trondheim, Norway. Attn: Professor J. K. Lunde.
3	Versuchsanstalt für Wasserbau und Schiffbau, Schleuseninsel im Tiergarten, Berlin, Germany. Attn: 1 - Dr. S. Schuster, Director 1 - Dr. H. Schwanecke 1 - Dr. Grosse
1	Technische Hogeschool, Institut voor Toegepaste Wiskunde, Julianalaan 132, Delft, Netherlands. Attn: Professor R. Timman.
1	Bureau d'Analyse et de Recherche Appliquees, 47 Avenue Victor Cresson, Issy-les-Moulineaux, Seine, France. Attn: Professor Siestrunck.
1	Netherlands Ship Model Basin, Wageningen, The Netherlands. Attn: Dr. Ir. J. D. van Manen.
2	National Physical Laboratory, Teddington, Middlesex, England. Attn: 1 - Mr. A. Silverleaf, Superintendent Ship Division 1 - Head, Aerodynamics Division
2	Head, Aerodynamics Department, Royal Aircraft Establishment, Farnborough, Hants, England. Attn: Mr. M. O. W. Wolfe.
1	Dr. S. F. Hoerner, 148 Busteed Drive, Midland Park, New Jersey.
1	Boeing Airplane Company, Seattle Division, Seattle, Washington. Attn: Mr. M. J. Turner.

Copies	Organization
1	Electric Boat Division, General Dynamics Corporation, Groton, Connecticut. Attn: Mr. Robert McCandliss.
1	General Applied Sciences Labs, Inc., Merrick and Stewart Avenues, Westbury, Long Island, New York.
1	Gibbs and Cox, Inc., 21 West Street, New York, New York.
3	Grumman Aircraft Engineering Corp., Bethpage, Long Island, New York. Attn: 1 - Mr. E. Baird 1 - Mr. E. Bower 1 - Mr. W. P. Carl
1	Lockheed Aircraft Corporation, Missiles and Space Division, Palo Alto, California. Attn: R. W. Kermeen.
1	Midwest Research Institute, 425 Volker Blvd., Kansas City 10, Missouri. Attn: Mr. Zeydel.
3	Director, Department of Mechanical Sciences, Southwest Research Institute, 8500 Culebra Road, San Antonio 6, Texas. Attn: 1 - Dr. H. N. Abramson 1 - Mr. G. Ransleben 1 - Editor, Applied Mechanics Review
2	Convair, A Division of General Dynamics, San Diego, California. Attn: 1 - Mr. R. H. Oversmith 1 - Mr. H. T. Brooke
1	Hughes Tool Company, Aircraft Division, Culver City, California. Attn: Mr. M. S. Harned.
1	Hydronautics, Incorporated, Pindell School Road, Howard County, Laurel, Maryland. Attn: Mr. Phillip Eisenberg.
1	Rand Development Corporation, 13600 Deise Avenue, Cleveland 10, Ohio. Attn: Dr. A. S. Iberall.
1	U. S. Rubber Company, Research and Development Department, Wayne, New Jersey. Attn: Mr. L. M. White.
1	Technical Research Group, Inc., 2 Aerial Way, Syosset, Long Island, New York. Attn: Mr. Jack Kotik.
1	Mr. C. Wigley, Flat 102, 6-9 Charterhouse Square, London, E. C. 1, England.
1	AVCO Corporation, Lycoming Division, 1701 K Street, N. W., Apt. 904, Washington, D. C. Attn: Mr. T. A. Duncan.
1	Mr. J. G. Baker, Baker Manufacturing Company, Evansville, Wisconsin.

Copies	Organization
1	Curtiss-Wright Corporation Research Division, Turbomachinery Division, Quehanna, Pennsylvania. Attn: Mr. George H. Pedersen.
1	Dr. Blaine R. Parkin, AiResearch Manufacturing Corporation, 9851-9951 Sepulveda Boulevard, Los Angeles 45, California.
1	The Boeing Company, Aero-Space Division, Seattle 24, Washington. Attn: Mr. R. E. Bateman (Internal Mail Station 46-74).
1	Lockheed Aircraft Corporation, California Division, Hydrodynamics Research, Burbank, California. Attn: Mr. Bill East.
1	National Research Council, Montreal Road, Ottawa 2, Canada. Attn: Mr. E. S. Turner.
1	The Rand Corporation, 1700 Main Street, Santa Monica, California. Attn: Technical Library.
2	Stanford University, Department of Civil Engineering, Stanford, California. Attn: 1 - Dr. Byrne Perry 1 - Dr. E. Y. Hsu
1	Dr. Hirsch Cohen, IBM Research Center, P. O. Box 218, Yorktown Heights, New York.
1	Mr. David Wellinger, Hydrofoil Projects, Radio Corporation of America, Burlington, Massachusetts.
1	Food Machinery Corporation, P. O. Box 367, San Jose, California. Attn: Mr. G. Tedrew.
1	Dr. T. R. Goodman, Oceanics, Inc., Technical Industrial Park, Plainview, Long Island, New York.
1	Professor Brunelle, Department of Aeronautical Engineering, Princeton University, Princeton, New Jersey.
1	Commanding Officer, Office of Naval Research Branch Office, 86 East Randolph Street, Chicago 1, Illinois.

ERRATA

The following corrections in Project Report No. 66 should be noted:

P. 51, line 8 - For "$\Delta P_{c_m}/\lambda$" substitute "$\Delta P_{c_m}/\gamma$".

P. 60 - For $V = 16$ fps, $f = 3$ in., and $\alpha = 10^{\circ}$, $\delta = 0^{\circ}$, (not 12°).

For $V = 16$ fps, $f = 3$ in., $c_f/c = 0.25$, $\alpha = 10^{\circ}$, and $\delta = 4^{\circ}$, values given for $W \times 10^3$ are in terms of lbs/sec rather than lbs/sec/in.^{2}

P. 62 - For $V = 16$ fps, $f = 3$ in., $\alpha = 14^{\circ}$, and $\delta = 0^{\circ}$ and for $V = 16$ fps, $f = 3$ in., $c_f/c = 0.25$, $\alpha = 14^{\circ}$, and $\delta = 4^{9}$, values given for $W \times 10^3$ are in terms of lbs/sec rather than lbs/sec/in.^{2}